HOTSSea v1: a NEMO-based physical Hindcast of the Salish Sea (1980 – 2018) supporting ecosystem model development

Greig L. Oldford[1,2], Tereza Jarníková [3], Villy Christensen[1], Michael Dunphy[4]

[1] Institute for Oceans and Fisheries, University of British Columbia, Vancouver, V6T 1Z4, Canada

5   [2] Ecosystem Sciences Division, Fisheries and Oceans Canada, Nanaimo, V9T 6N7, Canada

[3] Tyndall Centre for Climate Change Research, School of Environmental Sciences, University of East Anglia, Norwich, UK

[4] Institute for Oceans Science, Ocean Sciences Division, Fisheries and Oceans Canada, Sidney, V8L 5T5, Canada

10   *Correspondence to*: Greig L. Oldford (greig.oldford@dfo-mpo.gc.ca)

Abstract

Decadal-scale oceanographic, environmental, and ecological changes have been reported in the Salish Sea, an ecologically productive inland sea in the northeast Pacific that supports the economies and cultures of millions of people. However, there are substantial data gaps related to physical water properties that make it difficult to evaluate trends and the pathways of effects between physical ocean water properties and the productivity of marine ecosystems. With the aim of addressing these gaps, we present the Hindcast of the Salish Sea (HOTSSea) v1, a 3D physical oceanographic model developed using the Nucleus for European Modelling of the Ocean (NEMO) ocean engine, with temporal coverage from 1980 – 2018. We used an experimental approach to incrementally assess sensitivity to atmospheric and ocean reanalysis products used for boundary forcings and to the horizontal discretisation of the model grid (~1.5 km). Biases inherited from forcings were quantified and a simple temperature bias correction factor applied at one ocean boundary was found to substantially improve model skill. Evaluation of salinity and temperature indicates performance is best in the Strait of Georgia. Relatively large biases occur in near-surface waters, especially in sub-domains with topography narrower than the model grid's horizontal resolution. However, we demonstrated that the model simulates temperature anomalies and a secular warming trend over the entire water column in general agreement with observations. HOTSSea v1 provided a first look at spatially and temporally heterogenous ocean temperature trends throughout the northern and central part of the domain where observations are sparse. Overall, despite the biases inherited from forcings and a relatively coarse horizontal discretisation, HOTSSea v1 performs well at representing temperature and salinity at the spatial-temporal scales needed to support research related to decadal-scale climate effects on marine ecosystems, fish, and fisheries. We conclude by underscoring the need to further extend the hindcast to capture a regime shift that occurred in the 1970s.

Non-Technical Summary

We developed a 3D ocean model called the Hindcast of the Salish Sea (HOTSSea v1) that recreates physical conditions throughout the Salish Sea from 1980 to 2018. It was not clear that a model with sufficient accuracy could be developed because of computational and data limitations. However, HOTSSea v1 predicted physical ocean properties with enough skill to be highly useful. The model predictions generally agree with observed ocean temperature trends at the one rare station with observations and we therefore used it to examine areas that lack observations. Results indicate that some seasons and areas are warming faster than others.

Copyright

1. Introduction

The Salish Sea is an inland sea in the northeast Pacific spanning Canadian and American waters with estuarine characteristics, fjords, and high marine biodiversity (Harrison et al., 1983; Pata et al., 2022). The productive waters of the area support the economy and cultures of a rapidly growing coastal population of 8 – 10 million people including the port cities of Vancouver, British Columbia (BC, Canada), and Seattle, Washington (United States of America), and dozens of recreational, commercial, and indigenous fisheries (Georgia Strait Alliance, 2020). As global climate change unfolds and regional atmospheric and oceanographic regimes shift, within the Salish Sea there are seasonal, annual, and decadal-scale changes to physical oceanographic and atmospheric patterns that have been reported, including: changes in seasonal wind patterns (Collins et al., 2009; Masson & Cummins, 2007; Preikshot, 2007; Tuller, 2004), precipitation patterns (Beamish, 1993; Morrison et al., 2002; Yin et al., 1997), ocean water temperatures (Beamish et al., 2010; Masson & Cummins, 2007), properties related to ocean acidification (Feely et al., 2009; Ianson et al., 2016; Jarníková et al., 2022), and river discharge and temperatures (Islam et al., 2019; Martins et al., 2011; Riche et al., 2014). Increasing seasonal stratification and warmer surface waters may have increased the frequency and duration of harmful algal blooms (Esenkulova et al., 2021; Moore et al., 2015). Changes to regional climate patterns appear to have increased the variability of the date of the spring phytoplankton bloom (Allen & Wolfe, 2013) which may have led to spatial-temporal mismatches

between predators and prey (Allen & Wolfe, 2013; Suchy et al., 2022) and affected the composition of larval fish assemblages (Guan, 2015). Changing ocean conditions in the Salish Sea are also hypothesised to be affecting the abundance, composition, and spatial-temporal availability of prey for Pacific salmon via various pathways of effects (Pearsall et al., 2021). Several correlative studies link sea surface temperature and stratification with declining survival of several salmon species in the Salish Sea, particularly juvenile coho salmon (*Oncorhynchus kisutch*), Chinook salmon (*O. tshawytscha*), and steelhead (*O. mykiss*; Beamish, 1995; Pearsall et al., 2021; Perry, 2021; Sharma et al., 2013; Sobocinski et al., 2020, 2021; Walters & Christensen, 2019).

The patchy nature of oceanic data, particularly as we delve deeper into historical records within the Salish Sea, leads to uncertainty about the pace and spatial-temporal patterns of oceanographic change. Sparse observations also limit our ability to detect associations and evaluate mechanistic links between physical oceanographic changes and marine ecosystem dynamics. Physical oceanographic hindcasts are a pivotal tool for addressing such data gaps, offering a retrospective lens through which past oceanic conditions are reconstructed. Physical ocean models may also be coupled or linked to biogeochemical and ecosystem models using an 'End-to-End' approach useful for evaluating mechanistic drivers and dynamic pathways of effects between water properties, marine ecosystems, fisheries and other human uses (Libralato & Solidoro, 2009; Macias et al., 2014; Piroddi et al., 2021; Rose, 2012; Rose et al., 2010).

Although several oceanographic and biogeochemical models have been developed for the Salish Sea, attributes of these models presently limit their suitability for a long hindcast, including: computational cost due to high resolution and a focus on shorter term simulations (Jarníková et al., 2022; Khangaonkar et al., 2019; Olson et al., 2020; Soontiens et al., 2016; Soontiens & Allen, 2017), too coarse a resolution for use in the Salish Sea due to a focus on the wider BC coast (Peña et al., 2016), or a particular focus on Puget Sound (Khangaonkar et al., 2012, 2019; Khangaonkar, Nugraha, Lakshitha, et al., 2021; MacCready et al., 2021; Moore et al., 2015). It is therefore one aim of this study to develop a physical hindcast with a particular focus on the central and northern portion of the Salish Sea (i.e., the Strait of Georgia) with adequate spatial-temporal resolution to enable a long hindcast and acceptable model skill for supporting marine ecological research and ecosystem management. Although the acceptable model error will depend on the specific research question, ecological patterns and associated processes related to plankton and fish are often orders of magnitude greater than those required to study physical and chemical processes in marine ecosystems (Fulton et al., 2019). As a local example, hindcasting the timing of the spring phytoplankton bloom in the Strait of Georgia within an error margin of several days to one week at sub-regional scales is useful for studying spatial-temporal mismatches in predators and prey (Allen & Wolfe, 2013; Gower et al., 2013; Suchy et al., 2022). Many factors hypothesised to be mechanistically

linked to growth and mortality of juvenile salmon exhibit variability on time scales of one week or more and at spatial scales of >10 km (Pearsall et al., 2021). Another hinderance to development of a long hindcast for the area has been a lack of atmospheric and oceanic data extending back to at least 1980 to use as model forcings, and there are doubts about the adequacy of the few existing products with respect to spatial-temporal resolution. A second aim of this study is therefore to conduct experimental evaluation to identify biases inherited from external forcings (including some that only recently have been made available) to determine to what degree the available forcings limit the development of long oceanographic hindcasts in the area.

Here, we present HOTSSea v1, developed using the Nucleus for European Modelling of the Ocean (NEMO) Ocean engine (Madec et al., 2017). We describe and give rationale for the model setup with attention to three aspects that are particularly important for developing a long hindcast for the domain: (1) the biases inherited by using various atmospheric and ocean reanalysis products as surface and boundary forcing, (2) the effect of applying temperature bias corrections to the open ocean boundary forcing, and (3) a preliminary assessment of model performance relevant to the aforementioned research applications, including decadal-scale trends. Priority areas for improvement and further evaluation are also highlighted and, finally, we use the model to provide a first look at decadal-scale trends in the central and northern portion of the domain where historical observations are especially sparse.

2. Model Overview

The NEMO ocean engine, version 3.6, supports simulations of ocean dynamics and thermodynamic processes in three dimensions (Madec et al., 2017). The physical model framework is governed by primitive equations under hydrostatic balance using the Boussinesq approximation where density variations are neglected except in their contribution to the buoyancy force (Bourdallé-Badie et al., 2019). HOTSSea v1 was implemented in a high-performance computing cluster (*Digital Research Alliance of Canada*, 2022) and the model's scope is limited to physics and hydrodynamics (e.g., tides, salinity, temperature) - biogeochemistry is not included in HOTSSea v1 due to computational cost. We used state variables of Practical Salinity (PSU) and Potential Temperature (℃), and the EOS-80 equation of state (Millero, 2010). Sea ice is not included in HOTSSea v1 given that it occurs only occasionally in deep inland waters of fjords such as Jervis Inlet. To address issues of omitting ice, we applied NEMO's ice-if option, where the water temperatures are limited to the local salinity-dependent freezing point.

2.1. Spatial-Temporal Configuration
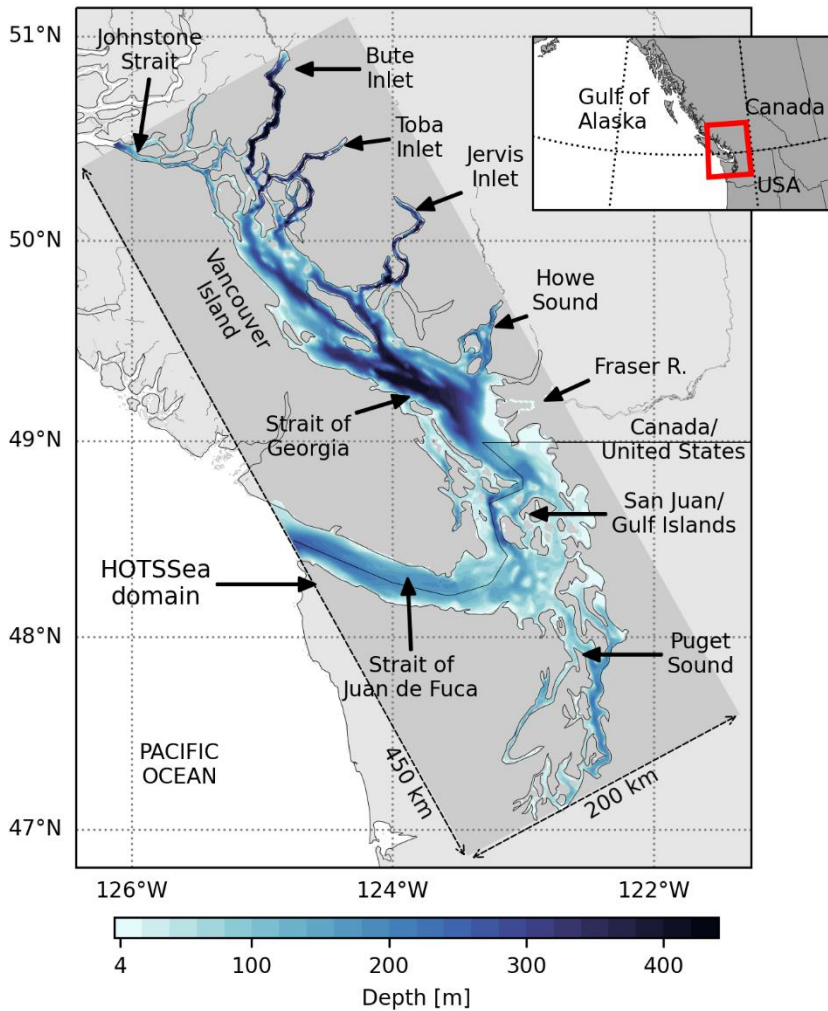
Figure 1: Map of model domain showing geographic features, extents of the HOTSSea NEMO model domain (medium grey), and bathymetry.

The model domain of HOTSSea v1 includes several distinct geographic areas within the Salish Sea: the Juan de Fuca Strait, Strait of Georgia, Gulf Islands, and Puget Sound (Figure 1). A key application of the model will be to provide forcings for biogeochemical and ecosystem models developed to investigate decadal-scale change. The model's spatial domain therefore fully encompasses the domain of an ecosystem model under parallel development that focuses on the Strait of Georgia and uses the Ecospace model framework (de Mutsert et al., 2023; Walters et al., 1999). To ensure the dynamics of the Strait of Georgia were resolved, it was deemed important to resolve the broader Salish Sea, with the connection to the open ocean via the Gulf Islands and the Juan de Fuca Strait being particularly important for resolving tides and estuarine flow (Ebbesmeyer et al., 1989; MacCready et al., 2021). The horizontal grid used in NEMO is discretised on a curvilinear orthogonal Arakawa C-grid generalised to three dimensions (Arakawa & Lamb, 1977; Madec et al., 2017). The basic spatial-temporal configuration of HOTSSea v1 began with a previous configuration,

SalishSeaCast, implemented at approximately 500 m horizontal resolution for the same domain (Olson et al., 2020; Soontiens et al., 2016; Soontiens & Allen, 2017). The ~500 m horizontal resolution grid and bathymetry used in the SalishSeaCast model was reduced by a factor of three in each horizontal direction, taking the mean depth of the neighbouring cells to assign the new depths.

155   The new grid is approximately 1.5 km in horizontal resolution and has a width of ~200 km and length of ~450 km (132 cells x 299 cells; Figure 1), which matches the grid and resolution of the Ecospace ecosystem model. The grid is rotated 29° counterclockwise to true north to align with the axis of the Strait of Georgia. The bathymetry was already processed for SalishSeaCast to avoid sudden changes in depths across grid cells and maintain open channels in narrow passages. We made additional

160   manual edits to maintain channels between islands, maintain connectivity of the main Fraser River channel to the outflow, and avoid erroneously isolating bodies of water. Some narrow water bodies such as Sechelt Inlet, Salmon Inlet, Burrard Inlet, and the Indian Arm fjord are not resolved in this setup (outlines of these areas are visible in Figure 1). The depths of edited channel cells were approximated from depth averages taken from ~80 m resolution bathymetric data (Pacific Salmon

165   Foundation, 2022). To ensure tidally-driven dynamics were not lost, the main channel of the Fraser River was extended inland by manually adding non-existent river channel cells approximately 150 km in total length, following Soontiens & Allen (2017).

The vertical grid for HOTSSea v1 is divided into 40 vertical (z) levels that are gradually stretched to achieve higher resolution at the surface, ranging from 1 m vertical resolution in the upper 10 m to

170   approximately 27 m widths at the deepest level (420 m). Partial steps were enabled to limit large changes in bathymetry between adjacent grid cells. The thickness of each layer is proportionally scaled at each time-step as sea surface height changes using a nonlinear free surface scheme referred to as the 'variable volume option' (Levier et al., 2007). HOTSSea v1 uses a non-linear free surface option to time-split the solving of the barotropic and baroclinic free surface. The barotropic

175   and baroclinic time steps are set to 6 s and 120 s, respectively, and the vertical momentum and tracer advection time stepping set to 2 s. The model was run from 1979-01-01 to 2019-01-01, where the 1980 atmospheric forcings were duplicated and applied to 1979, such that we treat 1979 as a model spin-up year and exclude it from evaluation. A one-year spin-up was based on a minimum estimate of deep water residency time which elsewhere has been reported to range between one and three years

180   (Pawlowicz et al., 2019). Initial conditions for January, 1979, for temperature and salinity across the domain were generated using climatologies for December and January using SalishSeaCast outputs from 2007 to 2020. An experimental bias correction to the ORAS5 temperature fields was applied when running the final hindcast.

2.2. Boundary Conditions and Forcings

Table 1: External forcing used in the model.

Forcing Dataset	Forcing Type	Model Runs	Temporal extent and resolution	Horizontal Resolution	Citation
Regional Deterministic Reforecast System (RDRS v2.1)	Surface / Atmospheric	Final	1980 – 2018; hourly	0.09°; ~10 km)	Gasset et al., 2021
European Centre for Medium-Range Weather Forecast (ECMWF) Ocean and Sea Ice Re-analysis v5 (ORAS5)	Open ocean boundary conditions	Final	1975 – 2018; monthly	0.25°; ~18 km	Tietsche et al., 2017; Zuo et al., 2019
Runoff / River Climatology and Gauge Data	Runoff	Final	1979 – 2018; hourly and daily	n/a	Morrison et al., 2012; Soontiens et al., 2016
Tidal Constituents	Tidal forcing at open boundaries	Final	n/a	n/a	Soontiens et al., 2016
Coastal Ice Ocean Prediction System (CIOPS) West	Open ocean boundary conditions	Evaluation	2007 – 2019; hourly	1/36°; ~2.5 km	Paquin et al., 2020
ECMWF ERA v5 (ERA5)	Surface / Atmospheric	Evaluation	1979 – present; hourly	0.28° ; ~31 km	Dee et al., 2011; Hersbach et al., 2020
High Resolution Deterministic Prediction System (HRDPS)	Surface / Atmospheric	Evaluation	2014 – 2020; hourly	0.0225°; ~2.5 km	Environment and Climate Change Canada, 2020

2.2.1. Atmospheric

The Regional Deterministic Reforecast System (RDRS v2.1; Gasset et al., 2021) supplied the
atmospheric conditions for forcing the full HOTSSea v1 hindcast. RDRS v2.1 is currently the highest
resolution atmospheric reanalysis product available extending back to 1980 (0.09°; ~10 km
horizontal). Two additional atmospheric forcings (Table 1) were evaluated as part of an experimental
design: the European Centre for Medium-Range Weather Forecasts (ECMWF) ERA5, a global
reanalysis product extending back to 1979 (hourly, at approximately 31 km horizontal resolution; Dee
et al., 2011; Hersbach et al., 2020) and the High Resolution Deterministic Prediction System
(HRDPS), with spatial coverage of the northern part of North America (Canada and northern United
States) with hourly coverage at ~2.5 km horizontal resolution for 2014 - 2020 (Environment and
Climate Change Canada, 2020). The RDRS v2.1 product occupies an intermediate horizontal
resolution between ERA5 and HRDPS, and the three together offered an opportunity to explore the
effect of horizontal resolution of atmospheric forcing on model performance in the Salish Sea.

2.2.2. Open Boundaries

There are two boundaries that connect the Salish Sea to the Pacific Ocean: the mouth of Juan de Fuca Strait in the southwest and Johnstone Strait in the north (Figure 1). To first evaluate the effects of using different ocean boundary forcings at the mouth of the Juan de Fuca Strait, a higher resolution model, CIOPS-West (Paquin et al., 2020), was used in shorter evaluation runs (horizontal resolution 2 - 2.5 km; 1/36°; Table 1,Table 2). The Ocean Reanalysis System 5 (ORAS5; Tietsche et al., 2017; Zuo et al., 2019) was the only available reanalysis product with coverage for the full model hindcast and was used to supply ocean open boundary conditions in the final model. ORAS5 has a horizontal resolution at the latitude of the Salish Sea of approximately 18 km (0.25°). At the northern boundary (Johnstone Strait), we used a monthly climatology of temperature and salinity (Dosser et al., 2020, 2021).

2.2.3. River Discharge and Runoff

River input into the Salish Sea periodically creates a brackish layer extending across the Strait of Georgia and drives strong estuarine circulation via Juan de Fuca Strait (Harrison et al., 1983). The Fraser River is the largest single source of freshwater influx into the domain and supplies approximately two thirds of the total annual freshwater input (Pawlowicz et al., 2019). Fraser River discharge is monitored as part of a long-term program (Morrison et al., 2012). Following Soontiens & Allen (2017), we used available flow records for the Fraser River from gauges approximately 150 km inland at the city of Hope, BC (Water Survey of Canada, 2015), and supplemented the Fraser River flow data with climatological data for additional freshwater input downstream of the station. A climatology was used for Fraser River runoff temperatures (Morrison et al., 2002) due to a lack of long-term measurements from the lower Fraser. The location of river outflow for the Fraser River was placed in the main channel before the river branches into a delta (at the town of Delta, BC). All other river outflows were assigned to the grid cell closest to the river mouth. Many rivers other than the Fraser are not monitored, so climatological patterns for discharge and temperature for 150 rivers flowing into the Salish Sea were used (Morrison et al., 2012). We adapted the input file containing these river input data from the ~500 m horizontal resolution model grid used by Soontiens et al. (2016) to the ~1.5 km horizontal resolution used here and adjusted the outflow locations as required.

2.2.4. Tides

At the two open boundaries, tides were forced with eight tidal constituents (K1, O1, P1, Q1, M2, K2, N2, and S2). Tidal heights and currents at the Juan de Fuca boundary were originally taken from WebTide (Foreman et al., 2000) and then manually tuned (Soontiens et al., 2016). At the northern

open boundary sea surface height and tidal harmonics were forced for the major M2 and K1 constituents and SSH harmonics for the O1 and S2 harmonics were configured using calculations from Thomson & Huggett (1980) with remaining constituents taken from WebTide and subsequently tuned.

3. Model Evaluation

Observations were collated from various instruments and sources (Table 2) and used to do a preliminary evaluation of the model's performance with respect to sea surface temperature (SST), sea surface salinity (SSS) and temperature and salinity over depths. To understand the trade-offs between spatial-temporal resolution, tractability, and model skill we used an experimental approach where forcings were incrementally swapped to help with isolating the most likely source of model error and bias. The NEMO-based SalishSeaCast model (v201905) outputs were used for comparison when evaluating the effect on overall model performance of changing the spatial-temporal setup, as we used this model as a foundation for the HOTSSea v1 model. As such, HOTSSea v1 shares limitations of the SalishSeaCast model, such as no wetting and drying capability in inter-tidal areas, climatologies used for river flow for all rivers except for the Fraser River, and biases in temperature and salinity. Aspects of SalishSeaCast's model skill with respect to physical properties have been previously reported (Olson et al., 2020; Soontiens et al., 2016; Soontiens & Allen, 2017). The mean temperature biases over all depths ranged from -0.21 to 0.13 °C and for depths less than 15 m were -0.34 to 0.36 °C, respectively (Olson et al., 2020). The mean salinity bias over the same two depth strata ranged from -0.74 to +0.23 PSU and -1.62 to 0.23 PSU, respectively (Olson et al., 2020). Our results may differ because the previous study did not necessarily use the same observational data nor did it use the subdomain definitions we used. For evaluation of temperature trends in the final hindcast, we used the modelled long-term temperature trend against observations at Nanoose station, the only long-term dataset with at least biweekly depth profiles done in the model domain extending back to the beginning of the hindcast (Table 2).

260   **Table 2:** Summary of data used for model evaluation.

Instrument Type	Dataset Title	Variables	Observations (N)	Description	Source
Conductivity, Temperature, and Depths (CTD) Casts	Fisheries and Oceans Canada's (DFO) Institute for Ocean Science (IOS) CTD casts dataset	Conductivity, Temperature, Depth, Pressure, Oxygen and Salinity	24,810	Contains CTD measurements collected in the Central Strait of Georgia, British Columbia, Canada using rosette mounted CTDs.	DFO, 2022c
	DFO IOS (including Nanoose Station)	Salinity, Temperature, Depth, Pressure	3,942	Surveys conducted from 1965 to present including Nanoose Bay station, a Canadian military CTD dataset which were provided upon request from DFO.	Personal communication (DFO) and WaterProperties.ca
	Hakai Institute	Salinity, Temperature, Depth, Pressure	2,871	CTD data collected from 2012 to present by the Hakai Institute in waters surrounding Calvert Island, Johnstone Strait, and Quadra Island areas.	Jackson et al., 2021
	Pacific Salmon Foundation (PSF)	Salinity, Temperature, Depth, Pressure	3,437	CTD casts collected by PSF for Strait of Georgia.	Pacific Salmon Foundation, 2023
Lightstation (LS) Near-Surface Water Properties	Environment and Climate Change Canada (ECCC)	Temperature, Salinity	7	Observations from lightstations where daily sea-surface temperature and salinity measurements have been collected from 1914 to present. Measurements were made daily using seawater collected in a bucket lowered into the surface water at or near the daytime high tide.	DFO, 2022a; Treasury Board Secretariat, 2023
Buoys	ECCC via DFO	Sea Surface Temperature (SST)	5	Wave and temperature data from buoys. Sea surface temperature data have undergone automated quality control. Historical data are merged with real-time acquisition.	Fisheries and Oceans Canada (DFO), 2024

3.1. Experimental Evaluation

The years chosen for running preliminary experimental evaluations were 2016 – 2018. The available
forcing data and models had coverage for those years and generally a larger volume of evaluation
data is available for the most recent years (Table 3). Experimental runs of the HOTSSea model were
given run codes. The first was HOTSSea v0.1, which used the highest resolution atmospheric and
ocean boundary forcings available. This run was used to do a comparative evaluation with
SalishSeaCast v201905 which has a higher horizontal resolution (~500 m versus ~1500 m). The
LiveOcean model (Fatland et al., 2016) forcings used in SalishSeaCast at the JFS open ocean
boundary were not available for the 2016 – 2018 period so in HOTSSea v0.1 we used CIOPS-W
BC12, a model also developed using the NEMO v3.6 ocean engine covering the northeast Pacific at
an approximate horizontal resolution of 2.0 - 2.5 km (Paquin et al., 2020). The HOTSSea v0.12
experiment was used to evaluate the effect of swapping from HRDPS to the ERA5 atmospheric
forcings (~31 km horizontal; Dee et al., 2011; Hersbach et al., 2020). At the time HOTSSea
development began in 2021, ERA5 was the only climate reanalysis product available for the entirety
of the hindcast period. At the time of writing, it is still the only reanalysis extending back to the 1940s
and therefore evaluation of this product for use for atmospheric forcing was a priority. The v0.14 and
v0.16 experiments jointly helped evaluate the effect of using the ORAS5 (~18 km horizontal; Tietsche
et al., 2017; Zuo et al., 2019) dataset for ocean boundary conditions at the mouth of Juan de Fuca
Strait, which will be used in the final hindcast; the two experiments used the lowest resolution
atmospheric forcings (v0.14; ERA5) and the highest resolution atmospheric forcings (v0.16; HRDPS)
to assist with isolating the effects on model performance of ORAS5 versus the atmospheric forcings.
The HOTSSea v0.18 experiment used the RDRS v2.1 atmospheric outputs for forcing, which have an
intermediate horizontal resolution of ~10 km (Gasset et al., 2021). To evaluate each experiment, we
used data, methods, and statistics as described in the next section. Model performance was
evaluated using results aggregated over the 2016 - 2018 period - analyses were also carried out on
model results grouped by month and year, though only results aggregated for the entire period are
presented here and only the results using CTD measurements are highlighted here for brevity.

Table 3: Experimental evaluation run codes and forcings.

Model	Version or Run Code	Evaluation Purpose	Years	Surface Forcing	Ocean Boundary Forcing	Reference
SalishSeaCast (~ 0.5 km)	v201905	Comparison of model performance at higher horizontal resolution	2016 – 2018	HRDPS	LiveOcean at JFS boundary, climatology at northern boundary	Soontiens et al., 2016; Soontiens & Allen, 2017; Olson et al., 2020
CIOPS-W	BC12	Comparison of model performance at lower horizontal resolution	2016 - 2018	HRDPS & RDPS[a] (~10 km)	Regional Ice Ocean Prediction System (RIOPS) v2	Paquin et al., 2020
HOTSSea (~1.5 km)	v0.1	Comparison with two models listed above using ~1.5 km^2 horizontal resolution	2016 - 2018	HRDPS	CIOPS-West	This study
HOTSSea	v0.12	Evaluate sensitivity to lower resolution atmospheric forcing	2016 - 2018	ERA5	CIOPS-West	This study
HOTSSea	v0.14	Evaluate sensitivity to lower resolution ocean boundary and atmospheric forcings	2016 - 2018	ERA5	ORAS5 (western boundary), climatology (northern boundary)	This study
HOTSSea	v0.16	Uses highest resolution atmospheric forcings available; evaluates sensitivity to lower resolution ocean boundary forcings	2016 - 2018	HRDPS	ORAS5 (western boundary), climatology (northern boundary)	This study
HOTSSea	v0.18	Uses the forcings used in the final model; evaluates sensitivity to intermediate resolution atmospheric and lower resolution boundary forcings	2016 - 2018	RDRS v2.1	ORAS5 (western boundary) and climatology (northern boundary)	This study
HOTSSea	v1.01	First full hindcast run	1979 - 2018	RDRS v2.1	ORAS5 (western boundary) and climatology (northern boundary)	This study
HOTSSea	v1.02	Full hindcast run with bias correction	1979 - 2018	RDRS v2.1	ORAS5 - temperature bias correction (western boundary) and climatology (northern boundary)	This study

* Approximate horizontal resolutions are included in brackets where not otherwise included in Tab. 1

[a] RDPS = Regional Deterministic Prediction System (used by CIOPS-W, not used herein)

3.2. Model-Observations Evaluation Methods

295
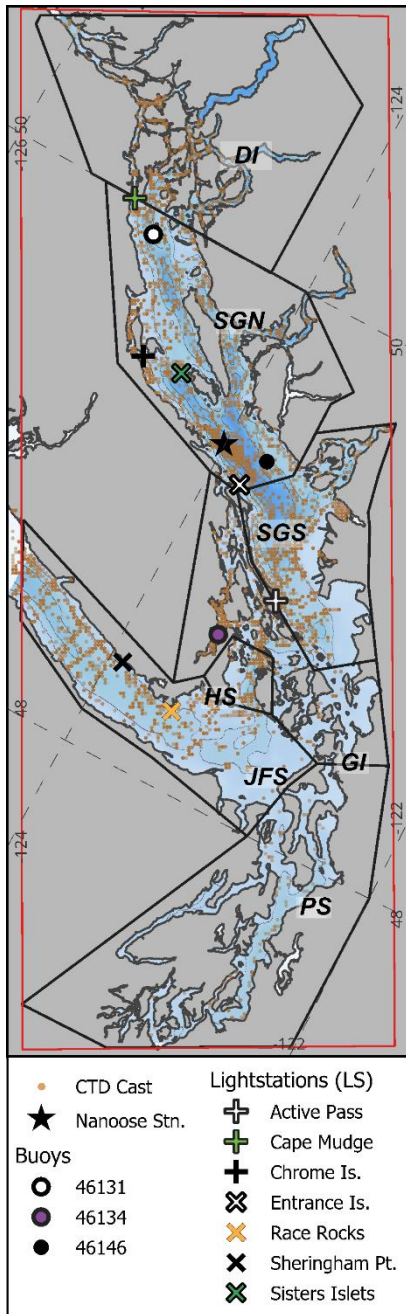
Figure 2: Map of HOTSSea v1 model domain (red rectangle) and subdomains used for analysis (black polygons; DI = Discovery Islands, SGN = Strait of Georgia North, SGS = Strait of Georgia South, HS = Haro Strait, GI = Gulf Islands, JFS = Juan de Fuca Strait, PS = Puget Sound). Locations of CTD casts are indicated by orange stippling (darker denotes higher density), and Nanoose station is indicated by the black star.

300

The final hindcast was evaluated using the datasets grouped by subdomains (Table 2, Figure 2).

305   Subdomains were selected based on distinct geographic features, data availability, and physical characteristics.

3.2.1. Vertical Profiles

CTD casts were acquired from various sources (Table 2). After quality control, 27,272 CTD casts were used in the analysis of the final hindcast. These data have heterogeneous spatial coverage

310   when aggregated by subdomain (Figure 2; Table 4). For the model intercomparison and experimental evaluation only CTD data from 2016 - 2018 were used ($N = 8,012$), which also had spatially heterogenous coverage across subdomain.

Table 4: Spatial distribution of CTD data used for evaluation of entire hindcast (1980 - 2018) and shorter experiments (2016

315   - 2018).

	CTD count	
Subdomain	**1980 - 2018**	**2016 – 2018**
Discovery Islands (DI)	3,649 (2.3 km^{-2})	1,884 (1.2 km^{-2})
Strait of Georgia North (SGN)	12,365 (2.9 km^{-2})	3,080 (0.7 km^{-2})
Strait of Georgia South (SGS)	4,140 (1.5 km^{-2})	1,517 (0.5 km^{-2})
Gulf Islands (GI)	2,512 (1.4 km^{-2})	871 (0.5 km^{-2})
Haro Strait (HS)	800 (2.0 km^{-2})	184 (0.5 km^{-2})
Puget Sound (PS)	99 (0.04 km^{-2})	23 (0.01 km^{-2})
Juan de Fuca Strait (JFS)	3,707 (0.9 km^{-2})	453 (0.1 km^{-2})
Total :	**27,272** (1.5 km^{-2})	**8,012** (0.4 km^{-2})

* brackets indicate spatial density of measurements

The closest model grid cell and time index was found for each CTD measurement and the measurements over depths for each CTD cast were vertically interpolated to the model depth levels. To calculate the statistics described below, CTD data were first grouped by subdomain, period, and

320   depth strata during analysis. We highlight in the subsequent sections only the results of grouping the data first by subdomain and model depth level and second by subdomain and selected depth strata (0 -> 30 m; 30 -> 150 m; > 150 m; and over all depths). For statistics grouped by depth strata, the depth-integrated mean from individual CTD casts within each depth grouping were first calculated. These values were treated as a single measurement (o_i) in the set of CTD casts, *N*, across each

325   subdomain with $\bar{o}$ representing the mean of depth-integrated means. Model results were extracted for each observation and depth-integrated in the same manner.

The model error was calculated for each model-observation pair (*m, o*) of time series (*Error = m – o*) with the bias being the mean error. The Root Mean Square Error (RMSE) was also calculated for each depth stratum, time frame, and subdomain. The bias and RMSE is often used to infer the

330   accuracy of a model whereas the Centred Root Mean Square Error (CRMSE) quantifies the precision (Walther & Moore, 2005), as the variability of the model as compared with observations as:

$$\text{CRMSE} = \sqrt{\frac{1}{N}\sum_{i=1}^{N}\left((m_i - \overline{m}) - (o_i - \overline{o})\right)^2} \tag{1}$$

where o_i denotes a single observation out of a set of observations, N, with the corresponding model output denoted by m_i. The Willmott Skill Score (WSS) was also used, a dimensionless measure of model skill ranging from zero denoting poor agreement between model and observations to one denoting perfect agreement (Willmott, 1981):

$$WSS = 1 - \frac{\sum_{i=1}^{N}(m_i - o_i)^2}{\sum_{i=1}^{N}(|m_i - \overline{o}| + |o_i - \overline{o}|)^2} \tag{2}$$

3.2.2. Sea Surface Temperature and Salinity

Sea surface temperature (SST) and salinity (SSS) were evaluated using measurements collected at high tide during daylight hours by lighthouse staff at seven lighthouses throughout the domain (Figure 2; Treasury Board Secretariat, 2023). Lightstation data (LS) were available for the entirety of the hindcast period for Chrome Island, Entrance Island, and Race Rocks lighthouses whereas others had partial coverage (Table 5). The time of day when samples were taken was not always provided in the dataset. As such, the closest tidal gauge each day was found for each lighthouse and the high tide time was extracted and then matched to the lighthouse sample data as required.

Table 5: Lightstation data summary used for evaluation of SST and SSS.

Lightstation ID	Years	Location (subdomain)
Active Pass	1980 – 2011	SGS
Cape Mudge	1980 – 1985	SGN
Chrome Island	1980 – 2019	SGN
Entrance Island	1980 – 2018	SGN
Race Rocks	1980 – 2018	JFS
Sheringham Point	1980 – 1988	JFS
Sisters Islets	1980 - 2008	SGN

Sea surface temperature measurements were also available from buoys within the model domain (Figure 2). Canadian buoy data were downloaded from online repositories (Fisheries and Oceans Canada (DFO), 2024; NOAA National Buoy Data Centre, 2023). The buoy data we prepared had heterogeneous temporal coverage of the hindcast period (Table 6). For the evaluation of the full hindcast we only used buoys with ten or more years of data (buoy IDs: 46146, 46131, 46134).

355 **Table 6:** Buoy data summary used for evaluation of SST.

Buoy ID	Years	Location (subdomain)
46131	1992 - 2019	SGN
46134	2001 - 2019	GI
46146	1992 - 2019	SGN

The statistics used for evaluation of SST and SSS include the standard deviation, σ, and Pearson's R (i.e., the corelation coefficient):

$$R = \frac{1}{\sigma_o \sigma_m} \frac{1}{N} \sum_{i=1}^{N} (m_i - \overline{m})(o_i - \overline{o}) \tag{3}$$

360   For plotting of results using Taylor diagrams, the σ_m and CRMSE statistics were normalised by scaling to the standard deviation of the observations to allow display of evaluation results for multiple stations on the same plots. The Normalised Centred Root Mean Square Error (NCRMSE) is computed using the relationship between σ, *R*, and *CRMSE*:

$$CRMSE = \sqrt{\sigma_o^2 + \sigma_m^2 - 2\sigma_o \sigma_m R} \tag{4}$$

365   thus,

$$NCRMSE = CRMSE / \sigma_o \tag{5}$$

and,

$$\sigma_m' = \frac{\sigma_m}{\sigma_o} \tag{6}$$

where σ_m' denotes the normalised standard deviation. Note that in target plots, the NCRMSE has been modified by the sign of σ_m - σ_o (Kärnä et al., 2021).

3.3. Ocean Boundary Temperature Bias Correction
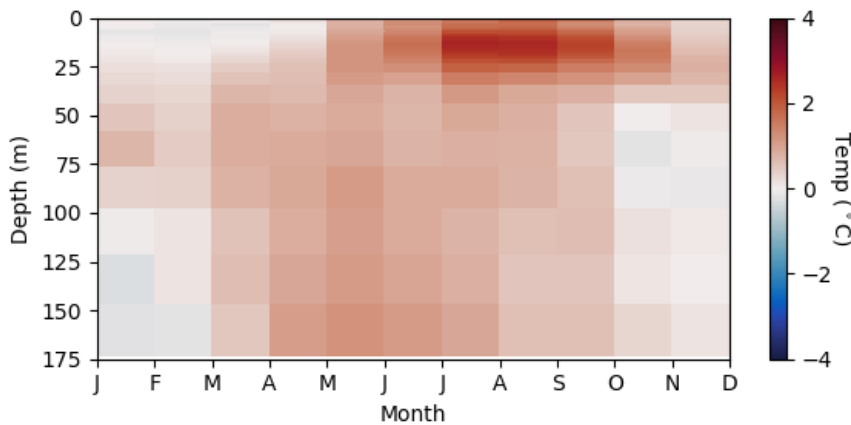
Figure 3: Monthly climatology of ORAS5 temperature bias over depths at Juan de Fuca open ocean boundary.

The ORAS5 global ocean reanalysis extends back to 1958 (Copernicus Climate Change Service, 2021) and it would be ideal to extend the model back to 1958, too; however, the magnitude of biases that would be inherited from ORAS5 was hitherto unknown. Based on the results of experiments (Table 3), we suspected biases could be substantial. To investigate, we collated observations from CTD instruments sampled between 1980 and 2018 from the mouth of the Juan de Fuca Strait (N = 2,162) and compared these observations to temperatures in the ORAS5 data. We chose to do this for the entire hindcast period rather than using the experiments for only 2016 - 2018 given the observational data available at this location for the experimental period were relatively limited. ORAS5 outputs were interpolated from monthly to daily using the *cdo* toolset (Schulzweida, 2022), which is the same procedure done by NEMO internal routines during model runs. Each CTD measurement was then matched to the closest ORAS5 grid point. Both the observations and the ORAS5 model data were interpolated vertically to the HOTSSea model depth levels. The ORAS5 model bias was calculated using monthly mean bias at each depth level.

The analysis indicated that ORAS5 at the JFS boundary is biased warm most depths and months except January with the mean summer bias near the surface approaching +4 °C (Figure 3). Surface waters in the ORAS5 model were biased fresh in the spring and summer, especially in the top 10 m where the mean bias approached -4 PSU. As a first step towards a more comprehensive bias correction, the mean monthly temperature bias for each depth level was used as a correction factor applied to the boundary conditions. We chose to prioritise temperature to isolate a single variable and because applying a bias correction factor to salinity would run a risk of introducing dynamic instability. The temperature bias correction method is acknowledged here to be a crude approach compared to various alternatives (Adachi & Tomita, 2020). The model run with ocean boundary temperature bias

correction factor applied to ORAS5 is referred to as HOTSSea v1.02. We then evaluated the change in model performance versus with no temperature bias correction (HOTSSea v1.01).

3.4. Trend Analysis

The ability of the HOTSSea model to recreate observed long-term ocean temperature trends is one of
400 the most important tests of the utility of the model. The only station in the model domain where
measurements over the entire water column were collected with bi-weekly regularity for the entirety of
the hindcast is the Nanoose station, located in the central Strait of Georgia (Figure 2). At this location,
CTD casts have been sampled approximately every two weeks since 1979 and with less regularity
back to the late 1960s. Trends in water temperature at Nanoose station were previously analysed and
405 estimated to be 0.24 +/- 0.1 ℃ decade^{-1} between 1970 and 2005 (Masson & Cummins, 2007; MC07).
We acquired the same Nanoose station data as analysed by MC07 with updates for recent years
from a digital archive at DFO Institute of Ocean Sciences (IOS) and in the DFO IOS Water Properties
Database in August, 2022. To cross-check our analysis with MC07, we also calculated the slope for
the same period as that study (1970 – 2005) similarly using ordinary least squares linear regression
410 and found a similar result: a warming trend over the water column (4.5 – 400 m) of 0.257 ℃ / decade
was assessed here versus 0.24 ℃ / decade in MC07. We attribute the difference to the application of
a boxcar filter in MC07 to the anomalies in the previous study.

To compare temperature anomalies and trends observed at Nanoose station with those predicted by
the model, first obviously erroneous measurements (e.g., with coordinates on land or depths
415 exceeding the maximum depth of ~400 m at Nanoose station) were removed and units were
converted to match those used in HOTSSea. The number of CTD casts ultimately used was 5,692.
Measurements taken in each CTD cast were interpolated to match the model depth levels of the
closest HOTSSea grid cell. The mean for each depth level grouped in two-week time intervals was
calculated for the hindcast period. A climatology over depth and time was generated for the hindcast
420 period by taking the mean across years for each depth level and two-week block. Time series of
temperature and salinity anomalies were calculated by differencing the depth-binned data and the
climatology. A 'blind' approach was then used to match each CTD cast to HOTSSea outputs where
model data were only extracted for dates, times, and locations corresponding to each CTD
measurement (i.e., gaps in the Nanoose time series also were present in the extracted model
425 results). The same procedure as above was then used for the model results to generate climatologies
and anomalies.

Analysis of temperature trends was conducted using the Nanoose station data and model results
drawn from the same area to examine the performance of HOTSSea v1.0x at simulating long-term
trends. Depths shallower than 4.5 m were omitted because the first depth at which measurements

were taken was inconsistent (following MC07). The analysis of the depth integrated anomaly trend over the entire water column (4.5 – 400 m) was first done, followed by analysis of the trend at each model depth. To quantify the magnitude of a linear trend, the Theil-Sen slope was used (TS; Sen, 1968; Theil, 1950). The TS approach is more robust to data gaps, outliers, and non-normal and heteroscedastic residuals than ordinary least squares linear regression (LR; Wilcox, 1998). To calculate TS, the median slope of all data pairs is found:

$$TS = median\left[\frac{x_i - x_j}{j - i}\right] \text{ for all i < j} \tag{7}$$

where (x_i, x_j) is a pair of values in the ordered time series ($j > i$). The LR method used in MC07 and the TS method were compared and we estimated the trend for the 1970 – 2005 period using TS to be 0.256 ℃ / decade, effectively the same as the LR method after accounting for measurement precision (see above). The similarity between trends estimated between the LR and TS method is consistent with findings in a previous analysis of SST in the same region (Amos et al., 2015).

Detrended residuals were analysed for periodicity, autocorrelation, non-normal distribution, and heteroskedasticity prior to choosing the test used for determining statistical significance. The data were first 'deseasoned' using the climatological mean to produce anomalies, as described above. The deseasoned anomalies were detrended by removing the secular trend calculated using the TS method and fast Fourier transform (FFT) was used to detect any remaining periodicities in the detrended and deseasoned residuals by examining the top five peaks in the power spectrum (Bluestein, 1970; Cooley & Tukey, 1965) using *scipy* (Virtanen et al., 2020) and *numpy* Python packages (Harris et al., 2020). The presence of autocorrelation was evaluated by modelling the residuals as a first order autoregressive process (AR-1) and computing the autocorrelation function (ACF) using Bartlett's method for computing the 95% confidence interval (Brockwell & Davis, 2016; Parzen, 1964) with the *statsmodels* package in Python (Seabold & Perktold, 2010). The residuals were tested for normality using the Shapiro-Wilk test where *p* value of <=0.9 was interpreted as insufficient evidence to reject a non-normal distribution (Shapiro & Wilk, 1965) using *scipy*. Heteroskedacity was evaluated using White's test (White, 1980) and the Goldfeld-Quandt test (Goldfeld & Quandt, 1965) using *statsmodels*.

The analysis using FFT revealed the presence of periodicity in residuals of frequencies of 5.1 and 17.7 years, confirming that the data were de-seasoned at the sub-annual scale but suggesting climate modes operating at longer time scales may limit the ability of accurate secular trend estimation, a similar result to previous studies (Amos et al., 2015). The 17.7 periodicity detected is consistent with the PDO, the NPGO, or a combination of the two. The 5 year period is approximately consistent with the ENSO cycle (Andres Araujo et al., 2013; McPhaden et al., 2006).

Analysis of the data revealed that the residuals of the detrended anomalies (both model and observation) had significant autocorrelation, were not normally distributed, and with some heteroskedasticity detected at some depths. The Mann-Kendall (MK) method (Kendall, 1948; Mann, 1945), a non-parametric method, was chosen for evaluating trend significance. This method is widely used in climatological and meteorological applications (Amos et al., 2015; Gocic & Trajkovic, 2013) and has the advantage of being relatively robust to non-normal data distributions and the data gaps present in the Nanoose time series. To check for statistical significance using MK, first the 'S' statistic is calculated:

$$S = \sum_{i=1}^{n-1} \sum_{j=i+1}^{n} sgn(x_j - x_i) \tag{8}$$

where n is the number of data points in the time series and $sgn(x_j - x_i)$ representing the sign function:

$$sgn(\theta) = \begin{cases} +1, if\ \theta\ >\ 0; \\ 0, if\ \theta\ =\ 0; \\ -1, if\ \theta\ <\ 0 \end{cases} \tag{9}$$

When the S statistic is greater than 0, it indicates that values earlier in the time series tend to be lower than those later and the trend therefore tends positive. Next, the variance of the test statistic is required, which accounts for ties in the data:

$$VAR(S) = \frac{1}{18}\left[n(n-1)(2n+5) - \sum_{p=1}^{m} t_p(t_p - 1)(2t_p + 5) \right] \tag{10}$$

where n is the length of the time series, m is the number of tied values, and t_p is the number of ties in the pth tied value. Using S and VAR(S), one computes the standardised normal variate Z:

$$Z_{MK} = \begin{cases} \dfrac{S-1}{\sqrt{VAR(S)}}, if\ S\ >\ 0; \\ 0, if\ S\ =\ 0; \\ \dfrac{S+1}{\sqrt{VAR(S)}}, if\ S\ <\ 0 \end{cases} \tag{11}$$

The standardised statistic, Z_{MK}, follows the normal distribution with $E(Z) = 0$ and $V(Z) = 1$. The null hypothesis – that there is no trend – may be rejected if the absolute value of Z is larger than the theoretical value of $Z_{1-\alpha/2}$ for a one-tailed test or $Z_{1-\alpha}$ for a two-tailed test (used here), where α is a chosen statistical significance level, which here was 95%. The Z values were also used for lower confidence limits (LCL) and upper confidence limits (UCL). The MK test, similar to LR with t-test, requires the data be independent and therefore serial autocorrelation must be dealt with in advance (Helsel & Hirsch, 1992). Yue et al., (2002) proposed a 'pre-whitening' procedure to remove the effect of serial autocorrelation prior to estimating the trend significance using MK. When autocorrelation was present, we used the '3PW' algorithm (Collaud Coen et al., 2020) which combines three pre-whitening methods to minimise risks of type I and type II errors which we applied using the *mannkendall* (v1.1.1) Python code.

After comparing the model with the measurements from the Nanoose dataset, we evaluated the trend in temperature and salinity for several depth strata (< 30 m, 30 - 150 m, > 150 m, and all depths) in each grid cell in the subdomain using the same statistical methods described above, though the 3PW method was not applied due to computational cost. The analysis was limited to the Strait of Georgia and surrounding waters for several reasons: (i) preliminary results indicated that model performance was best in this part of the domain, (ii) observations collated have relatively more coverage in this area, (iii) and it is the focus of an ecosystem model under development in parallel. Mean weekly water temperatures were calculated for each grid cell, season ('winter' = December, January, February; 'spring' = March, April, May, 'summer' = June, July, August; 'fall' = September, October, November), and for each depth group. When generating plots, grid cells were masked that were shallower than a threshold set for each depth strata (thresholds: 20 m for 0->30 m; 150 m for 30->150 m; 200 m for >150 m) and coloured grey.

4. Results

4.1. Experimental Evaluation
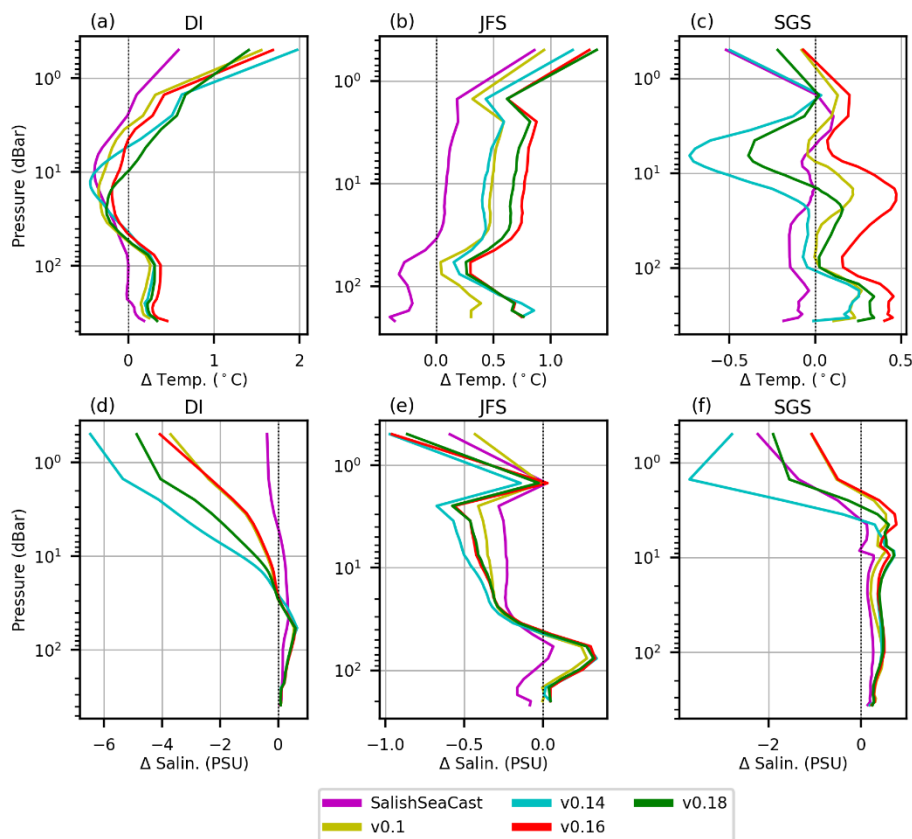
Figure 4: Model bias (model - observations) over depths using CTD data for short (2016 - 2018) experimental runs, highlighting temperature (top row) and salinity (second row) bias and CRMSE over depths (shading). HOTSSea v0.18 corresponds to the setup used in the final model run without bias correction (v1.01). v0.12 was omitted from the plots as results were nearly identical to v0.14. See Fig. 2 for map of subdomains.

In the first model experiment (years 2016 – 2018), HOTSSea v0.1 experiment was compared with the higher resolution SalishSeaCast model. A notable difference was that v0.1 had a mean bias taken over all depths of 0.14 °C in the SGS subdomain versus -0.017 °C in SalishSeaCast (Figure 4c). Large differences were noted in the northernmost DI subdomain where near-surface (0 - 1.5 m) biases were larger in v0.1 relative to SalishSeaCast, approaching +2 °C and -4 PSU at 0.5 m (Figure 4a,d). We attribute the warm bias in the DI subdomain to the 3x coarsened HOTSSea model grid relative to SalishSeaCast, limiting the model's ability to resolve the relatively narrow topography in the DI. At depths > 1.5 m HOTSSea v0.1 performed well, even in the DI, with mean biases over the water column of -0.12 °C and -0.4 PSU. In the JFS subdomain, HOTSSea v0.1 performed similarly to SalishSeaCast except for the introduction of a temperature bias of 0.3 - 0.5 °C at depths > 2 m, with the bias most pronounced at depths > 20 m (Figure 4b). A similar bias was also present in the Strait of Georgia South (SGS) subdomain (Figure 4c). The boundary forcings were hypothesised to be the

main culprit, since different boundary forcings were used here (CIOPS-W) than in SalishSeaCast (LiveOcean).

520

The v0.12 and v0.14 experiments were designed to evaluate the effect on the model's performance of using relatively coarse atmospheric forcings from ERA5 (~31 km horiz. res.) versus the relatively highly resolved HRDPS (~2.5 km horizontal) forcings used in v0.1. The v0.12 and v0.14 experiments used different ocean boundary forcings, though the resulting salinity and temperature biases over
525 depths were indistinguishable between the two (which prompted us to remove v0.12 from Figure 4). The similarities suggest that any performance impacts of using ORAS5 (~18 km horiz.) versus CIOPS-W (~2.5 km horiz. res.) were masked by the relatively greater impacts of using coarse ERA5 atmospheric forcings. Among all experimental runs, v0.12 and v0.14 had the greatest near-surface biases in temperature and salinity in the northern part of the model domain (i.e., DI subdomain;
530 Figure 4a,d). and in the central part of the domain (i.e., SGS domain; Figure 4c,f). We investigated possible reasons and diagnosed that winds in ERA5 are generally weak and less variable throughout the domain relative to the higher resolution HRDPS winds.

The HOTSSea v0.16 experiment helped isolate and evaluate the effect of using ORAS5 for boundary
535 conditions at the Juan de Fuca Strait open ocean boundary versus the relatively highly resolved CIOPS-W. In the northern-most subdomain, the Discovery Islands (DI), v0.16 showed similar biases to v0.14 with respect to salinity and temperature over depths (Figure 4a,d). Looking to the SGS subdomain in the central part of the model domain, a relatively large warm bias appeared in v0.16 at depths greater than 10 m (approximately +0.3 °C at 10 m depth, increasing to +0.5 °C at 100+ m
540 depths; Figure 4c). In the JFS subdomain closest to the open ocean boundary, the biases in temperature at depths > 5 m were greater in v0.16 than in the other subdomains and greater relative to previous experimental runs, with biases of > 1 °C near the surface and +0.4 to +0.75 °C at greater depths (Figure 4b). The v0.16 experiment's performance with respect to salinity in JFS were comparable to v0.14 (Figure 4e). Our interpretation of these results is that in v0.16 the model
545 inherited a warm bias in mid and deep waters from the ORAS5 boundary conditions, evidenced by decreasing temperature bias with increasing distance from the open ocean boundary. Contrary to expectations, using the *lower* resolution ERA5 atmospheric forcings in the HOTSSea v0.14 experiment resulted in *less* of a warm temperature bias across all depths in the JFS subdomain at depths up to 100 m and had little discernible effect on salinity as compared with results of using the
550 *higher* resolution HRDPS outputs for atmospheric conditions in the v0.16 experiment. The better performance of v0.14 in JFS was unexpected because the model domain is relatively poorly resolved by ERA5 versus HRDPS. We suspect that wind-driven vertical mixing is biased low when using ERA5 and therefore ERA5 masks the effect of a near-surface warm bias introduced by ORAS5 by keeping

the biased-warm water closer to the surface. Further investigation is warranted and understanding the
555   sources of biases is a priority.

In the final experimental run, HOTSSea v0.18, the RDRS v2.1 (~10 km horizontal) atmospheric
conditions were used, representing an intermediate between the highest resolution HRDPS forcings
available only for 2014 - 2020 and the lower resolution ERA5 forcings available for the entire hindcast
560   period. The run performed similarly or better than the previous two runs with respect to temperature
and salinity in most subdomains. The JFS subdomain was an exception where the warm temperature
bias was greater than in v0.14 (Figure 4b). As above, the increased temperature bias was
unexpected since v0.14 used the relatively weak and poorly resolved ERA5 atmospheric conditions.
Thus, using both higher resolution and presumably more accurate atmospheric products (RDRS and
565   HRDPS) resulted in *greater* temperature bias over depths up to ~80 m in the JFS subdomain. This
result is consistent with the diagnosis we reached earlier that the ERA5 atmospheric forcing fields
used in the v0.14 experiment masked the effects of a warm temperature bias in the JFS subdomain
up to depths of ~10 m due to weaker winds and a shallower mixing as compared to the more powerful
HRDPS and RDRS winds in the v0.14 and v0.18 experiments, respectively.
570

The preliminary experiments illuminated several important factors affecting model performance
related to atmospheric and ocean boundary forcings. Coarsening the model bathymetry from 500 m
to 1.5 km horizontally has especially impacted model performance in areas with narrow topography
when compared with SalishSeaCast, but otherwise has had only a minor effect on the evaluated
575   aspects of model performance. Puget Sound (PS) remains essentially unevaluated (though see
Tables S1, S2) due to a lack of collated data for the area but we suspect similar issues to the DI
subdomain due to narrow topography; expanding our evaluation to PS remains a priority for future
work. An important takeaway was an apparent systemic temperature bias present in ORAS5, the only
reanalysis for hindcasting the ocean boundary conditions to 1980 and prior available at the time of
580   writing. The ERA5 product similarly was deemed to be inadequate for the present purposes due to
underpowered winds throughout the domain (RDRS v2.1 was used instead). The experiments
prompted us to verify and quantify the bias introduced at the ocean boundary and to determine if
simple bias correction could hold potential to reduce or eliminate inherited biases (results below).

4.2. Bias Correction of Open Ocean Boundary Conditions
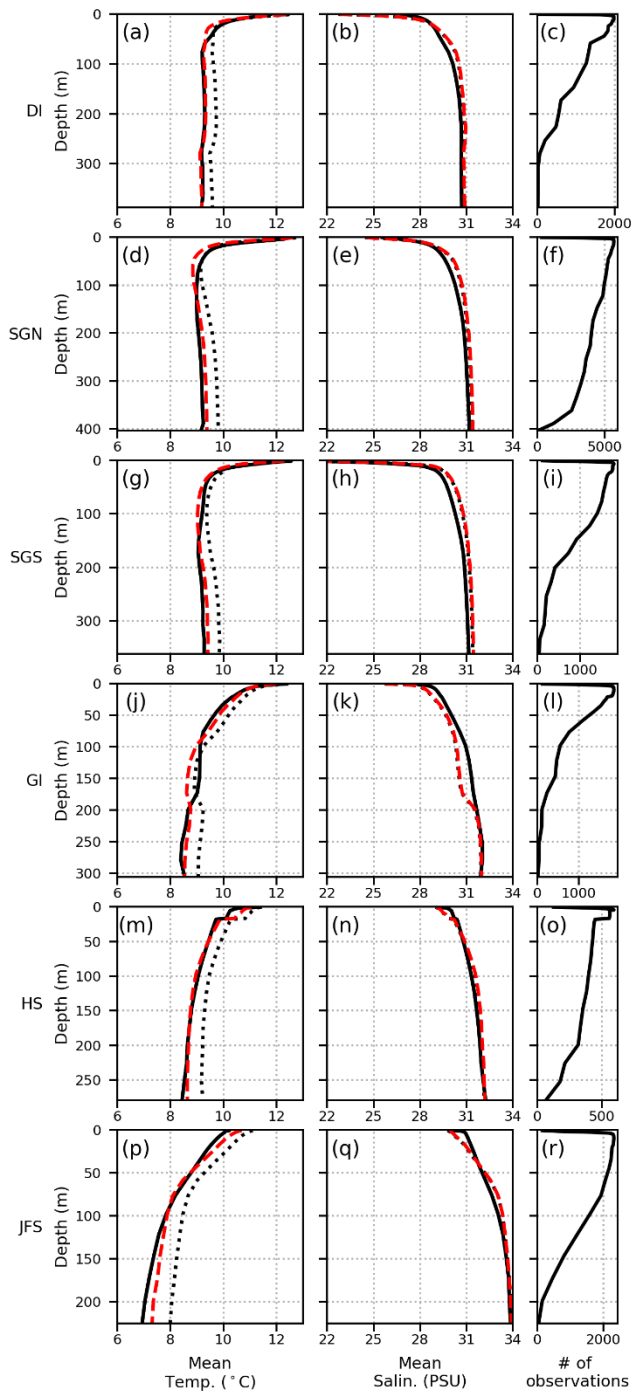
585

Figure 5: Results of analysis using CTD data, aggregated by subdomain, showing mean temperature and salinity over depths (solid line = observations, dashed black line = HOTSSea v1.01 without bias correction, dashed red line = HOTSSea v1.02 with bias correction)
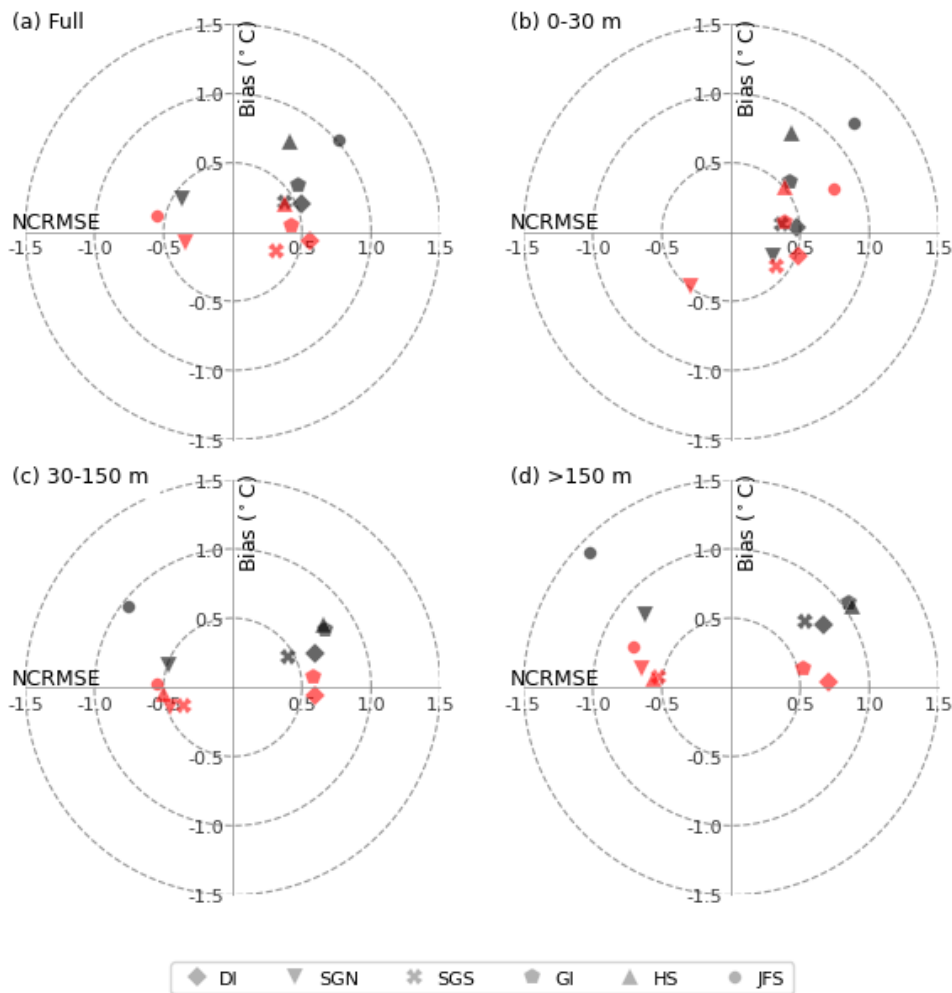
Figure 6: Target plots of the model's temperature bias and normalised centred root mean squared error (NCRMSE) using CTD data grouped by depth strata (panels a - d) and by subdomain. Results without bias correction to western open ocean boundary conditions (HOTSSea v1.01) are shown in grey and results with temperature bias correction (HOTSSea v1.02) are shown in red.

595   The effect of the temperature bias corrections applied in HOTSSea v1.02 substantially improved model skill versus v1.01 (Figure 5,6; Tables S1,S2). In the JFS subdomain, for example, temperature bias calculated over all depths was reduced from +0.66 to +0.12 ℃. The HOTSSea v1.01 run without bias correction had mean temperature biases calculated over all depths of +0.21 to +0.66 ℃ (excluding the PS subdomain with sparse observations) versus -0.14 to +0.2 ℃ in HOTSSea v1.02

600   (Table S1). Applying the temperature bias correction improved the model's performance in the most distant subdomain from JFS, the DI subdomain – an unexpected result that emphasises the importance of accurate ocean boundary forcings.

4.3. Model-Observation Evaluation

4.3.1. Vertical Profiles

Overall, the full hindcast (HOTSSea v1.02) performs best in the central and northern portion of the domain (Figure 5). In the SGN subdomain where the most CTD casts were available (N = 12,288), the temperature bias over all depths over the hindcast period was –0.08 ℃ (0 - 30 m = -0.39 ℃, 30 - 150 m = -0.14 ℃, > 150 m = +0.13 ℃) with overall WSS of 0.97 and correlation coefficient (R) of 0.94 (Tables S1, S2). Performance was similar in the SGS subdomain. The normalised target and Taylor diagrams (Figure 6, S1-S3) indicate the model captures the seasonal ocean temperature variability well, though NCRMSE was > 0.5 for JFS in the west and DI subdomains in the north. Model standard deviation is generally higher than observations in shallow depths and lower in deep water. Except for JFS and DI subdomains, the mean correlation coefficient with respect to temperature taken over all depths was >0.9 (Figure S1a; Table S1). As depths increase, correlation generally decreases. At depths greater than 150 m, the model underestimates temperature variability and the correlation coefficient was <0.8 for DI, JFS, and SGN. The southernmost PS subdomain was omitted from analysis due to relatively few observations collated and preparing data for this area is a priority for future work. All metrics are tabulated by subdomain and depth strata in Tabs. S1 and S2 for reference.

HOTSSea v1.02 model skill was relatively poor with respect to salinity compared with temperature, especially in the DI and JFS subdomains (Table S2; Figures S2-S3). However, performance was better in the Strait of Georgia where mean bias taken over all depths in the SGS subdomain was +0.38 PSU (WSS =0.98 and R=0.96; Table S2). The narrow topography in the DI combined with the 1.5 km horizontal resolution is likely leading to the observed error, as evidenced by experiments (Figure 4). Another reason for salinity biases to increase in subdomains farther from the Fraser River could be that a climatology is used for estimating input from other rivers in the domain, whereas measurements are available for the Fraser River (Morrison et al., 2012). The open ocean boundary conditions are forced using a climatology at the northern boundary in the DI subdomain and this would be affecting model skill. However, the latter two explanations are considered less likely given the same boundary climatology and river forcings were used here as were used in SalishSeaCast which performs well in the DI subdomain (Figure 4).

4.3.2. Sea surface temperature and salinity
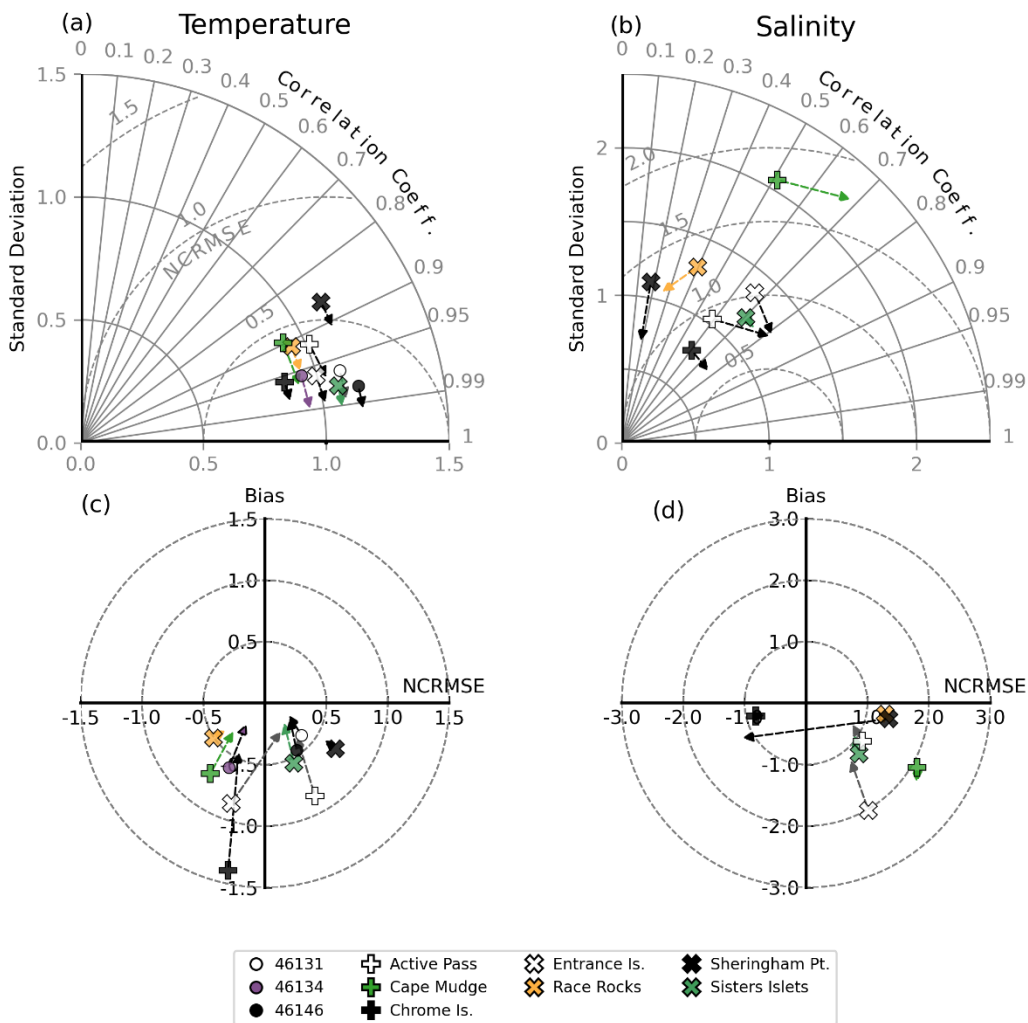
Figure 7: Taylor (top) and target (bottom) plots evaluating HOTSSea v1.02 sea surface temperature (SST; left) and salinity (SSS; right). SST was evaluated using data from buoys (numbered) and lightstations (named) and SSS was evaluated using lightstation data only. Standard deviation (solid grey contours in Taylor diagrams) and centred root mean square error (dashed grey contours in Taylor diagram) have been normalised to enable comparison on the same plot. Perfect agreement between model and observations on the Taylor plot would correspond to normalised standard deviation = 1, correlation = 1, and NCRMSE = 0. Perfect agreement between model and observations on the target plot would be at the centre. Arrows depict the change after applying a one month moving average on both the model and observation time series.

Time series of SST and SSS taken at lightstations in the region are some of the longest in existence and present a valuable opportunity to evaluate model performance. SST and SSS were evaluated for the full hindcast using data from sampling at lightstations and buoys with temporal coverage of at least ten years. The Taylor plots indicate the model reproduces the variability in SST well (Figure 7a). Most stations have NCRMSE < 0.5 with a correlation coefficient greater than 0.9. HOTSSea v1.02 performs well at stations within the Strait of Georgia and relatively poorly Sheringham Pt in the Juan de Fuca Strait where the standard deviation of the model is approximately 20% higher than observations. The normalised target diagram (Figure 7c), shows that the model is typically biased

cold with the mean bias typically < 0.75 ℃. The one lightstation with >1 ℃ bias was Chrome Island which is located on an island close to shore where bathymetry is poorly resolved.

The evaluation of SSS indicates that HOTSSea v1.02 typically overestimates variability in SSS across the domain, as the normalised standard deviation of the model is greater than the
655   observations at all stations except Chrome Island (Figure 7b). Although the model's performance with respect to SST is better than SSS, the model's normalised standard deviation for SSS at all stations except Cape Mudge deviated by less than +/- 30% of the observations. The correlation coefficient for SSS at most stations was relatively poor (0.4 - 0.7) compared to SST (>0.85). The target plot indicates that the model is biased fresh at the surface by approximately -1 PSU at Cape Mudge in the
660   northern part of the domain and -2 PSU at Entrance Island in the central Strait of Georgia, whereas at other stations the fresh bias was relatively small (< -1 PSU; Figure 7d).

Many applications of HOTSSea v1 in support of ecosystem modelling and research related to Pacific salmon are anticipated to require accuracy at weekly, monthly, or seasonal time scales rather than daily or hourly. To investigate whether the lower SSS performance was due to difficulty capturing
665   dynamics over hourly or daily time scales versus longer time scales, we applied a monthly moving average to both the model and observations after which statistics were recalculated. Applying the moving average improved the evaluated statistics at all stations except Sheringham Point (Figure 7, arrows). The improvement leads us to conclude that if research applications require bias < 0.5 ℃ or < 1.0 PSU then averaging results to monthly may be ensure the accuracy is acceptable with respect to
670   SST and SSS. As shown in Sect. 4.3.1, the model performance generally improves with depth.

4.4. Decadal temperature trend evaluation

4.4.1. Nanoose station
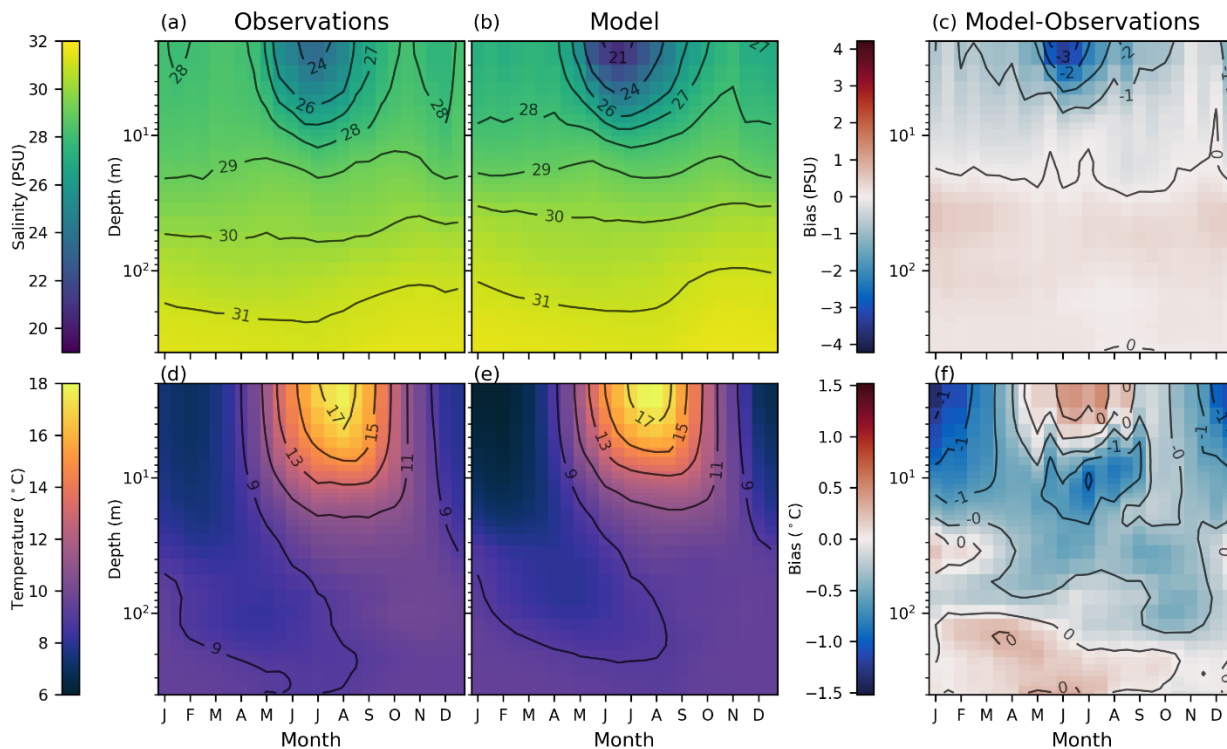
Figure 8: Biweekly climatologies and model-observation bias over depths over the hindcast period using measurements taken at Nanoose station between 1980 and 2018 ($N = 5,692$). The four panels to the left show salinity (top row) extracted from observations (first column) and the model (second column). Temperatures are similarly represented from observations and the model in the bottom plots. The two plots on the right show the model bias (i.e., model - observations) over depth. Data were binned bimonthly.

The model represents seasonal changes in salinity and temperature over depths well. Both the modelled and observed biweekly climatologies at Nanoose station depict a characteristic intrusion of cold water and a temperature inversion that occurs in the area in the spring and late summer or fall (Figure 8d,e), typically associated with upwelling events and neap tides (Johannessen et al., 2014; Masson, 2002; Riche et al., 2014). Strongly stratified and warm surface layers are shown in the shallower layers in the summer in both climatologies from the observations and from the model. The model-observation biases are generally largest at depths less than 3 m for both temperature and salinity. Although at depths >10 m there is only minor bias with respect to salinity (< 0.5 PSU), salinity is biased fresh in depths <3 m, especially in the summer when it approaches -3 PSU (Figure 8c). The fresh bias observed here is not surprising; it was also apparent in the higher resolution SalishSeaCast model (e.g., Figure 4f; Soontiens & Allen, 2017) which formed the basis for HOTSSea; however, it remains an important area for improvement in the future and may be affecting model skill with respect to circulation patterns. The modelled temperatures are biased warm in the summer and cool in the

winter by a maximum of approximately 1 °C at depths less than 3 m. In contrast, the modelled temperatures are consistently biased slightly high (~0.5 ℃) at depths over 100 m.

After truncating the Nanoose station time series to match the model hindcast period, the monotonic temperature trend across depths 4 – 400 m was calculated using the MK test and the TS slope estimator. Significant autocorrelation was detected in the detrended biweekly time series so the 3PW algorithm was used to adjust for this (see Sect. 3.4). The trend from observations at Nanoose station evaluated to be 0.031°C per decade (LCL: -0.018, UCL: 0.08; *p* <= 0.12). HOTSSea v1.01 *without* ocean boundary temperature bias correction detected no trend (0.00 °C / decade; LCL: -0.06, UCL: 0.06; p <= 0.73). The HOTSSea v1.02 *with* ocean temperature bias correction predicted a non-zero but insignificant trend of 0.012 °C per decade (LCL: -0.052, UCL: 0.075; *p* <= 0.3). Although trends over the water column for the 1980 – 2018 hindcast period were not significant at the 95% confidence level, results suggested that HOTSSea v1.02 with ocean boundary temperature bias correction performs better than HOTSSea v1.01 with respect to long term-trends.
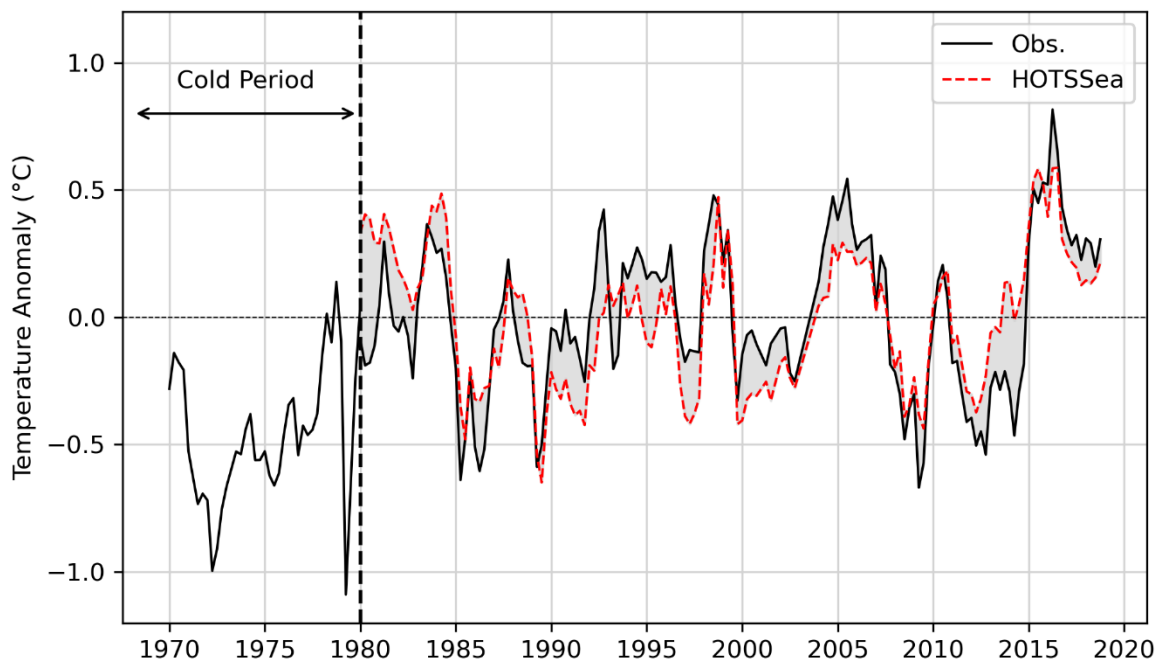
Figure 9: Temperature anomalies (seasonal) from observations (black, solid) at Nanoose station in the central Strait of Georgia versus those derived from HOTSSea v1.02 model outputs (red, dashed), depth integrated over 4.5 m - 400. The grey area represents the model bias. Observations from the 1970 – 1980 period at Nanoose are included to illustrate the cooler period, a multiyear swing in temperature anomalies (1977,1978), followed by a regime shift occurring circa 1977 (Beamish et al., 1999; Hare & Mantua, 2000).

The observed inter-annual and intra-annual variability over the hindcast period is well captured by the model (Figure 9). The largest deviations between modelled (HOTSSea v1.02) and observed temperature anomalies over the whole water column were < 0.5 °C. Relatively large deviations from observations in the 1980 – 1983 period suggest that the one-year spin-up may be too short and this remains a priority area to investigate in the future. Warm anomalies as a result of a documented

oceanic heat wave circa 2015-2016 (Gruber et al., 2021; Khangaonkar, Nugraha, Yun, et al., 2021) are generally well represented, suggesting the model is capable of reproducing extreme events. The evaluation of the trends at Nanoose station also indicate the model does not incur a detectable drift in temperature bias at this location, despite being run with no data assimilation.

720

The secular trend previously calculated for the 1970 to 2005 period of 0.24 °C per decade (95% CI ±0.1 °C; Masson & Cummins, 2007) was over 6-fold greater than calculated here for the 1980 to 2018 hindcast period. We verified that the difference was not attributable to the methods (TS vs. LR for slope estimation) by re-estimating the trend from the observations using LR for the same 1980 – 2018

725 period, finding a similar result using LR (0.038 °C / decade). The weaker secular trend calculated for the 1980 – 2018 period is in part due to the omission of the 1970s, a period with cold water temperature anomalies observed at Nanoose station (Figures 9, S4). The late 1970s corresponds approximately to a polarity shift in the Pacific Decadal Oscillation (PDO; Mantua et al., 1997; Mantua & Hare, 2002), a trough in the North Pacific Gyre Oscillation (NPGO; Di Lorenzo et al., 2008), which

730 oscillate on decadal or multi-decadal time scales. The late 1970s also corresponds to a trough in a multi-regime index circa 1977 that correlates with a reduction in Northern Pacific fisheries catches (Beamish et al., 1999). Overall, the analysis reveals a key limitation of HOTSSea v1 – omission of the 1970s – which is thus a priority area for subsequent iterations. Our analysis also serves as an update to the MC07 analysis and confirms ocean temperatures have not subsequently reverted.

735
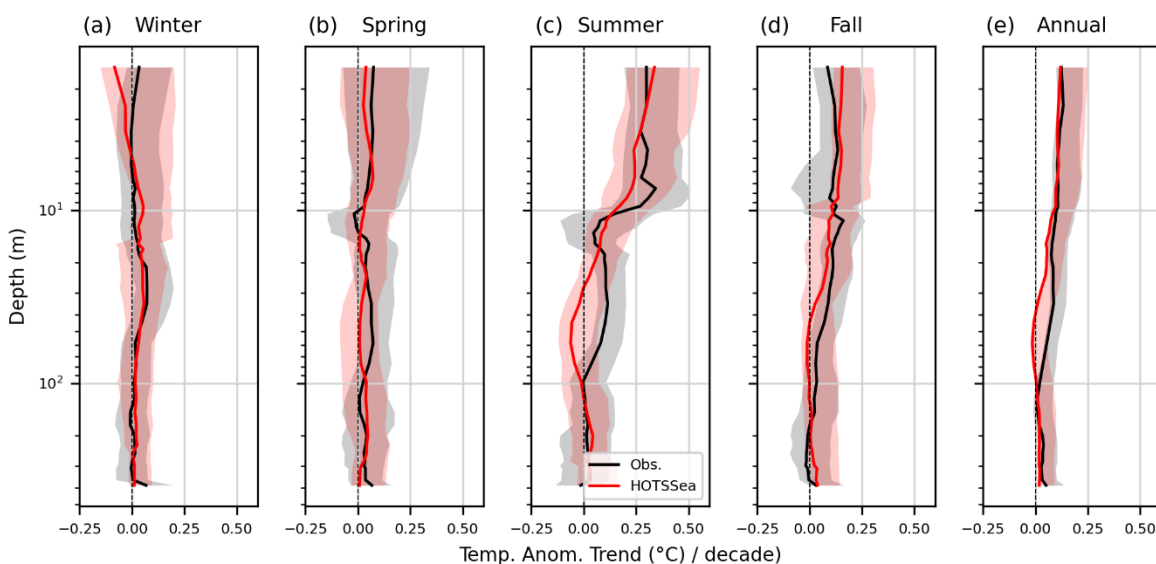
Figure 10: Seasonal and annual trends (1980-2018) over depths observed at Nanoose station compared with HOTSSea v1.02 outputs. Shading represents upper and lower 95% confidence limits.

Analysis of trends at each depth at Nanoose station indicate that the modelled trends are in generally

740 good agreement with observed trends (Figure 10). Both the modelled and observed seasonal trends in the upper water column in the summer, fall, and annually were statistically significant whereas the

trends in the winter and spring were not. A deviation between the modelled and observed trends is apparent, especially in the summer, between approximately 20 m and 100 m. The reason for the deviation is yet to be determined but a similar deviation is also apparent in the analysis using CTDs in the GI subdomain (Figure 5). The seasonal trend patterns over depth at Nanoose station indicate that trends vary seasonally and spatially (over depths) at this location.

4.4.2. Strait of Georgia
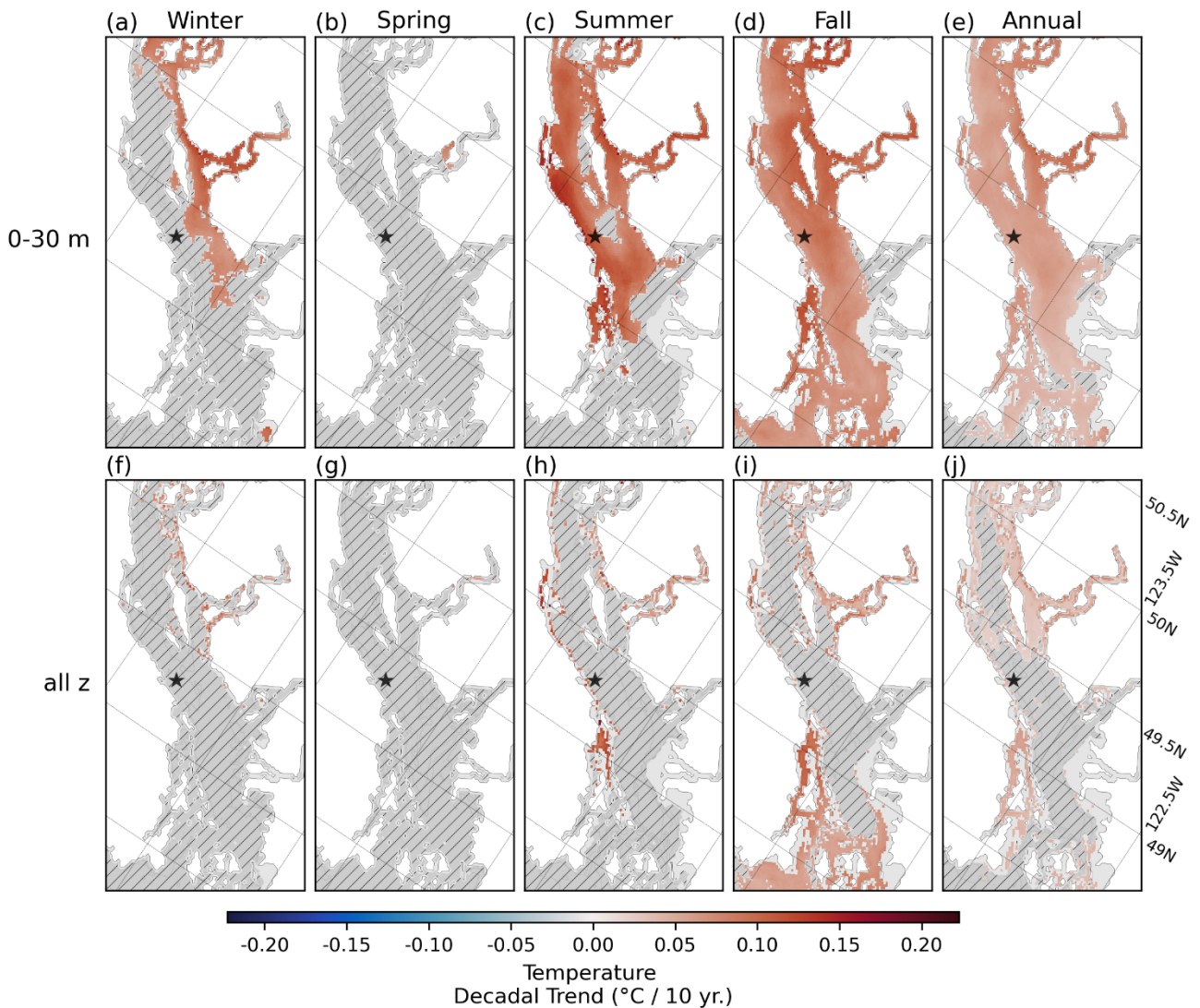
Figure 11: Mean ocean temperature trends in the Strait of Georgia computed as seasonal mean trends (columns) for two depth strata (rows): 0 – 30 m depth stratum and over all depths ('all z'), from HOTSSea v1.02 model outputs. Mask (grey) has been applied to grid cells that are shallower than the depth stratum. Grey hatching has been applied to grid cells where trend was not statistically significant. Star symbol denotes approximate location of Nanoose station.

Modelled trends from HOTSSea v1.02 were evaluated in each grid cell in the central and northern part of the model domain (Strait of Georgia and surrounding waters) over the 1980 – 2018 hindcast period (Figure 11). The 0 – 30 m depth stratum was selected given that the evaluation of the

modelled versus observed trends showed generally good agreement in approximately the top 30 m of the water column. This stratum also has special relevance for phytoplankton bloom dynamics (Allen & Wolfe, 2013). The model indicates the top 30 m are generally warming in the Strait of Georgia, with some areas experiencing statistically significant warming over the entire water column. Despite finding that the mean trend computed across all depths at Nanoose station in the winter was not statistically significant (Figure 10a, 11f), a statistically significant warming trend in the winter *was* detected in the 0-30 m depth stratum in the northeastern Strait of Georgia and in Jervis Inlet (Figure 11a). The rapid warming of Jervis Inlet is a finding consistent with trends reported for other fjords in the region (Jackson, Bianucci, et al., 2021). The analysis of temperature trends in the spring revealed no significant warming trend (Figure 11b), similar to the analysis of the Nanoose data (Figure 10b). In the summer, only the waters in the central and northern Strait of Georgia generally showed a statistically significant warming trend whereas the southern Gulf islands and surrounding waters showed no statistically significant trend (Figure 11c). The fall season may also have experienced the most spatially consistent secular ocean temperature warming since 1980 over the 0 – 30 m depth range - significant trends in the fall were generally widespread apart from Howe Sound (Figure 11d). Annualised trends were relatively low but generally statistically significant throughout the Strait of Georgia (Figure 11e). Note that the magnitude of all modelled trends throughout the domain are likely biased low, as the analysis of the modelled secular trend at Nanoose was weak relative to observed (see above).

5. Discussion and Conclusion

To our knowledge, HOTSSea v1 represents the first 3D physical oceanographic model for the Salish Sea to be extended back to 1980, as well as the first model to use recently available forcing products to do so (e.g., RDRS v2.1, ORAS5). A highlight of the results of our evaluation of HOTSSea v1 was the skill with which the model represents observed decadal-scale ocean temperature trends at Nanoose station - without incurring any detectable drift despite being a free run with no data assimilation (Figure 9, 10). After confirming the model's skill at recreating the trend at Nanoose station, we used the model to further our understanding trends in areas within the central and northern part of the domain with sparse observations, offering a first glimpse at the spatial-temporal heterogeneity of ocean temperature trends in the area (Figure 11). The 0 – 30 m depth range was of particular interest because changes occurring at these depths may particularly affect dynamics of spring and fall phytoplankton blooms (Masson & Peña, 2009). Most importantly, HOTSSea v1 outputs indicate that the warming trend apparent at Nanoose station is not an isolated phenomenon within the Salish Sea. Gradual ocean temperature changes such as those quantified by our analyses have the potential to affect the growth, body mass, and marine distributions of fish (Pauly, 2021; Pauly &

Cheung, 2018) and support research related to the 'velocity' of climate change (Burrows et al., 2014; Loarie et al., 2009). Anomalous events such as marine heatwaves are expected to occur more frequently due to climate change and these events can lead to key biophysical thresholds being surpassed, impacting marine organisms (Gruber et al., 2021). Given that HOTSSea v1 generally replicates observed ocean temperature anomalies and extremes it therefore shows promise for investigating climate-related pathways of effects from physical ocean properties to marine ecosystems.

Overall, our evaluation quantifies the biases of the model at several spatial-temporal scales with special attention to those scales and variables anticipated to be relevant for marine ecosystem model development, marine ecosystem research, and ecosystem-based fisheries management. Although variability in physical conditions at fine spatial-temporal scales (i.e., minutes to days, metres to kilometres) is an important determinant of the structure and dynamics of marine ecosystems (e.g., Jones et al., 2014), many research applications related to marine ecosystems focus on processes and mechanisms that exhibit variability on weekly or greater time scales and at spatial scales of 10's of km (Fulton et al., 2019). Locally, juvenile salmon enter the marine environment from natal rivers over a protracted period of weeks to months (Groot & Margolis, L., 1991; Healey, 1980), migrate at rates of 1.5 - 20 km day^{-1} (Melnychuk et al., 2010, 2013; Trudel et al., 2009; Tucker et al., 2009; Welch et al., 2011), are widely distributed throughout the pelagic zone (Beamish et al., 2011; Riddell et al., 2018; Trudel & Tucker, 2013), and exhibit weekly, monthly, and seasonal variability in growth and mortality. We therefore expect that hindcasting physical ocean water properties at the spatial-temporal resolution used here will be of value for many studies related to Pacific salmon.

A contemporary challenge to achieving a long hindcast for the Salish Sea is related to the quality of the available products to use for boundary and atmospheric forcing. The experimental approach we used helped us isolate the effect of forcings and our model's horizontal resolution from other factors affecting model performance, revealing substantial biases inherited from both atmospheric and oceanic boundary forcings. What we learned using this approach will guide future efforts to improve and extend HOTSSea v1 and possibly other models for the domain. Using the RDRS v2.1 forcings in the final hindcast led to substantially better model performance versus using ERA5 (Sect. 4.1) - presently the only alternative to our knowledge with coverage of the full hindcast period. Wind speed biases in ERA5 have been noted in other coastal and mountainous areas (Potisomporn et al., 2023). The results of our experiments similarly indicated that locally weak winds in ERA5 resulted in reduced mixing and increased near-surface biases, leading to especially poor model performance in areas with complex and narrow topography (e.g., the Discovery Islands). Winds are an important factor determining total productivity of the Strait of Georgia (Collins et al., 2009; Johannessen et al., 2020) and thus it was fortunate that the RDRS v2.1 atmospheric reanalysis was recently made available.

The experiments also revealed that the global ocean reanalysis ORAS5 outputs exhibit temperature and salinity biases at the mouth of the Juan de Fuca Strait which were inherited to some extent by our model. We suspect the main issue is that the Salish Sea is poorly resolved in ORAS5, leading to poor representation of estuarine flow and physical dynamics at the mouth of Juan de Fuca Strait. The temperature bias correction we applied here to ORAS5 at the Juan de Fuca boundary improved model performance substantially, even in areas of the domain far from the ocean boundary (Figures 5, 6). The success of our crude bias correction serves to highlight the potential benefit of relatively advanced techniques such as statistical downscaling using machine learning or the application of data assimilation techniques to produce a re-analysis (Adachi & Tomita, 2020). Another avenue worth exploring would be to use outputs from other regional ocean hindcasts as boundary forcings, should they become available (e.g., Paquin et al., 2020; Peña et al., 2016). Applying bias correction to salinity at the boundary could also be of benefit and may help with improving the model's near-surface fresh bias.

Next steps include several improvements, extensions, and applications. Our preliminary evaluation of the model prioritised the Juan de Fuca Strait and the central part of the Salish Sea (i.e., the Strait of Georgia and surrounding waters) whereas Puget Sound remains essentially unevaluated (though see Tables S1,S2). Collated Canadian observations had relatively sparse coverage of Puget Sound (Figure 2, Table 2) and adding more observations from American institutions therefore is a near-term priority. The reported biases in the final model are also a priority to diagnose and correct, especially near-surface fresh biases in summer months (e.g., Figure 8c), a bias that HOTSSea v1 shares with its predecessor, SalishSeaCast (Figure 4; Olson et al., 2020; Soontiens & Allen, 2017). The salinity bias is of particular concern as it may hinder the model's capability of representing circulation patterns. Evaluation of tides and the estuarine circulation is a particularly important task, as these are primary factors affecting deepwater renewal in the Salish Sea (Ebbesmeyer et al., 1989; MacCready et al., 2021). Once circulation is evaluated, one potentially promising application would be to use velocity fields from HOTSSea v1 for Lagrangian particle simulations (Hernández-Carrasco et al., 2020; Snauffer et al., 2014). Changes to regional scale atmospheric patterns may have affected sea surface height and circulation patterns which in turn may affect important ecosystem processes such as larval dispersal. A logical next step is to use data assimilation to combine information from dynamical simulation with observations to produce a reanalyses, with estimates for the oceanic fields that are maximally consistent with observations (Zaron, 2011). Data assimilation techniques are developing rapidly and show great promise for helping minimize model error. Finally, upgrading from NEMO v3.6 to NEMO v4.x is a priority, as new vertical mixing options and a wetting-and-drying scheme for intertidal areas hold potential for improving model skill in this domain (Madec et al., 2023).

Ultimately, we hope to extend HOTSSea further back in time, motivated by a need to capture the period prior to an oceanic regime shift that occurred circa 1977 that can be seen in the Nanoose station time series (Figure 9, S4). The regime shift is of particular interest for fisheries related research in the area (Beamish et al., 1999; Di Lorenzo et al., 2008; Mantua et al., 1997; Mantua & Hare, 2002; MC07). Despite various climate regime indices subsequently reverting in polarity, ocean temperatures may not have reverted. Coupling the physical model with a biogeochemical module is another potentially valuable avenue to explore, as integrating biogeochemistry into the hindcast would provide retrospective details of oxygen, nutrients, carbonate chemistry, aragonite saturation, and pH – all of which have changed since pre-industrial times in the Salish Sea (Jarníková et al., 2022). Secular ocean warming and increased seasonal variability have also had a quantifiable effect on oxygenation of deep fjord waters in the region (Jackson, Bianucci, et al., 2021) which may have affected the productivity or community composition of lower trophic levels (Johannessen et al., 2020). However, computational cost associated with traditional biogeochemical models are currently a challenge that would need to be overcome. The HOTSSea v1 reconstruction of temperature fields over depths should also prove useful for investigating the relative impact of pathogens and predation on fish. Warming ocean temperatures lead to greater vulnerability to pathogens and disease and thus to greater vulnerability to predation (Miller et al., 2014; Teffer et al., 2018), but concurrent increases in predator abundances make it difficult to determine whether predation is a primary or secondary mortality factor (Walters & Christensen, 2019). Available observational time series are mainly limited to surface waters and HOTSSea v1 can help address this gap by providing ocean temperature fields at specific depths and areas occupied by fish.

In conclusion, HOTSSea v1 shows promise for improving our understanding of long-term physical changes occurring in the Salish Sea with relevance for fish, fisheries, and marine ecosystems. The model's performance with respect to salinity, temperature, decadal scale trends, and temperature anomalies indicates HOTSSea v1 can support ecosystem research focused on dynamics that unfold over months, seasons, years, or decades. The model addresses significant gaps in historical observations and can help drive biogeochemical and ecosystem models aimed at revealing dominant drivers of ecological productivity (Hermann et al., 2023; Macias et al., 2014; Piroddi et al., 2021).

Author Contribution Statement

All authors contributed to the review and editing of the paper. GO wrote the original draft, conducted data preparation, analysis, formal evaluation, and data visualisations. MD did server configuration, compilation, and running of the model with contributions from GO. TJ provided expertise and carried out analyses related to trend analysis and climatologies. VC and MD contributed to the administration and supervision of the model development.

Acknowledgements

Financial support for GO was provided by the Natural Sciences and Engineering Research Council of Canada (NSERC) Mitacs program (#IT12313), Fisheries and Oceans Canada (Government of Canada), the Pacific Salmon Foundation, the University of British Columbia (UBC), and the UBC Ocean Leaders Program. This research was supported by the Salish Sea Marine Survival Project. The authors thank Susan Allen, Andrew Edwards, and Carl Walters for review and suggestions on drafts of the manuscript and extend thanks to Elise Olson for early discussions about analysis and code. The authors also acknowledge the work of Susan Allen and colleagues who developed the SalishSeaCast model for the same domain which served as the starting point for the HOTSSea v1 model.

Code and Data Availability

HOTSSea is based on the NEMO source code version 3.6 (Madec et al., 2017; subversion trunk revision rev10584), released under the open source CeCill license (https://cecill.info, last access: March 7, 2024). The standard NEMO source code can be downloaded from the NEMO website (http://www.nemo-ocean.eu, last access: March 7, 2024). The HOTSSea v1 configuration files and source code used for analysis and visuals in the present article has been archived at https://doi.org/10.5281/zenodo.12520931 (Oldford, 2024b). Forcings and observations prepared for the model are provided separately due to space limits, with HRDPS at https://zenodo.org/doi/10.5281/zenodo.12193923 (Oldford & Dunphy, 2024a); RDRS at https://zenodo.org/doi/10.5281/zenodo.12206290 (Oldford & Dunphy, 2024b); ERA5, CIOPS, runoff, and observational data at https://zenodo.org/doi/10.5281/zenodo.12312768 (Oldford & Dunphy, 2024c). Raw outputs are currently stored on a server without necessary bandwidth to make them publicly available given the file sizes; however, they can be made available by contacting the authors. Depth-averaged, monthly mean outputs are available online at https://zenodo.org/doi/10.5281/zenodo.13871970 (Oldford, 2024a). Processed versions of these outputs have been included in the 'pacea' open-source R package which aims to reduce the burden of wrangling such data for fisheries stock assessments and other applications (Edwards et al., 2024).

Competing Interests

925   The authors declare no competing interests.

References

Adachi, S. A., & Tomita, H. (2020). Methodology of the Constraint Condition in Dynamical

930   Downscaling for Regional Climate Evaluation: A Review. *Journal of Geophysical Research: Atmospheres*, *125*(11), e2019JD032166. https://doi.org/10.1029/2019JD032166

Allen, S. E., & Wolfe, M. A. (2013). Hindcast of the timing of the spring phytoplankton bloom in the strait of Georgia, 1968-2010. *Progress in Oceanography*, *115*, 6–13. https://doi.org/10.1016/j.pocean.2013.05.026

935   Amos, C. L., Martino, S., Sutherland, T. F., & Al Rashidi, T. (2015). Sea Surface Temperature Trends in the Coastal Zone of British Columbia, Canada. *Journal of Coastal Research*, *300*, 434–446. https://doi.org/10.2112/JCOASTRES-D-14-00114.1

Andres Araujo, H., Holt, C., Curtis, J. M. R. R., Perry, R. I., Irvine, J. R., Michielsens, C. G. J. J., Araujo, H. A., Holt, C., Curtis, J. M. R. R., Perry, R. I., Irvine, J. R., & Michielsens, C. G. J. J.

940   (2013). Building an ecosystem model using mismatched and fragmented data: A probabilistic network of early marine survival for coho salmon Oncorhynchus kisutch in the Strait of Georgia. *Progress in Oceanography*, *115*, 41–52. https://doi.org/10.1016/j.pocean.2013.05.022

Arakawa, A., & Lamb, V. R. (1977). Computational design of the basic dynamical processes of the

945   UCLA general circulation model. *General Circulation Models of the Atmosphere*, *17*(Supplement C), 173–265.

Beamish, R. J. (1993). Climate and Exceptional Fish Production off the West Coast of North America. *Canadian Journal of Fisheries and Aquatic Sciences*, *50*(10), 2270–2291. https://doi.org/10.1139/f93-252

950   Beamish, R. J. (1995). Climate Change and Northern Fish Populations. In *Canadian Special Publication of Fisheries and Aquatics Sciences* (Vol. 121, p. 754). National Research Council of Canada.

Beamish, R. J., Lange, K. L., Neville, C.-E. M., Sweeting, R. M., & Beacham, T. D. (2011). Structural patterns in the distribution of ocean- and stream-type juvenile chinook salmon populations in

955   the Strait of Georgia in 2010 during the critical early marine period. *North Pacific Anadromous Fish Commission*, *1354*(October), 27p.

Beamish, R. J., Noakes, D. J., McFarlane, G. A., Klyashtorin, L., Ivanov, V. V., & Kurashov, V. (1999). The regime concept and natural trends in the production of Pacific salmon. *Canadian Journal of Fisheries and Aquatic Sciences*, *56*(3), 516–526. https://doi.org/10.1139/f98-200

960 Beamish, R. J., Sweeting, R. M., Lange, K. L., Noakes, D. J., Preikshot, D. B., & Neville, C. M. (2010). Early Marine Survival of Coho Salmon in the Strait of Georgia Declines to Very Low Levels. *Marine and Coastal Fisheries*, *2*(1), 424–439. https://doi.org/10.1577/C09-040.1

Bluestein, L. (1970). A linear filtering approach to the computation of discrete Fourier transform. *IEEE Transactions on Audio and Electroacoustics*, *18*(4), 451–455. IEEE Transactions on Audio

965   and Electroacoustics. https://doi.org/10.1109/TAU.1970.1162132

Bourdallé-Badie, R., Bell, M., Chanut, J., Clementi, E., Coward, A., Drudi, M., Éthé, C., Iovino, D., Lea, D., Lévy, C., Madec, G., Martin, N., Masson, S., Mathiot, P., Mocavero, S., Müller, S., Nurser, G., Samson, G., & Storkey, D. (2019). *Nucleus for European Modelling of the Ocean: NEMO ocean engine* (p. 273). https://doi.org/10.5281/zenodo.1464816

970 Brockwell, P. J., & Davis, R. A. (2016). *Introduction to Time Series and Forecasting*. Springer International Publishing. https://doi.org/10.1007/978-3-319-29854-2

Burrows, M. T., Schoeman, D. S., Richardson, A. J., Molinos, J. G., Hoffmann, A., Buckley, L. B., Moore, P. J., Brown, C. J., Bruno, J. F., Duarte, C. M., Halpern, B. S., Hoegh-Guldberg, O., Kappel, C. V., Kiessling, W., O'Connor, M. I., Pandolfi, J. M., Parmesan, C., Sydeman, W. J.,

975   Ferrier, S., … Poloczanska, E. S. (2014). Geographical limits to species-range shifts are suggested by climate velocity. *Nature*, *507*(7493), 492–495. https://doi.org/10.1038/nature12976

Collaud Coen, M., Andrews, E., Bigi, A., Martucci, G., Romanens, G., Vogt, F. P. A., & Vuilleumier, L. (2020). Effects of the prewhitening method, the time granularity, and the time segmentation on

980   the Mann–Kendall trend detection and the associated Sen's slope. *Atmospheric Measurement Techniques*, *13*(12), 6945–6964. https://doi.org/10.5194/amt-13-6945-2020

Collins, A. K., Allen, S. E., Pawlowicz, R., Collins, A. K., Allen, S. E., & Pawlowicz, R. (2009). The role of wind in determining the timing of the spring bloom in the Strait of Georgia. *Canadian Journal of Fisheries and Aquatic Sciences*, *66*(9), 1597–1616. https://doi.org/10.1139/F09-071

Cooley, J. W., & Tukey, J. W. (1965). An Algorithm for the Machine Calculation of Complex Fourier Series. *Mathematics of Computation*, *19*(90), 297–301.

Copernicus Climate Change Service. (2021). *ORAS5 global ocean reanalysis monthly data from 1958 to present* [Dataset]. ECMWF. https://doi.org/10.24381/CDS.67E8EEB7

de Mutsert, K., Coll, M., Steenbeek, J., Ainsworth, C., Buszowski, J., Chagaris, D., Christensen, V., Heymans, S. J. J., Lewis, K. A., Libralato, S., Oldford, G., Piroddi, C., Romagnoni, G., Serpetti, N., Spence, M. A., & Walters, C. (2023). Advances in spatial-temporal coastal and marine ecosystem modeling using Ecospace. In *Reference Module in Earth Systems and Environmental Sciences*. Elsevier. https://doi.org/10.1016/B978-0-323-90798-9.00035-4

Dee, D. P., Uppala, S. M., Simmons, A. J., Berrisford, P., Poli, P., Kobayashi, S., Andrae, U., Balmaseda, M. A., Balsamo, G., Bauer, P., Bechtold, P., Beljaars, A. C. M., van de Berg, L., Bidlot, J., Bormann, N., Delsol, C., Dragani, R., Fuentes, M., Geer, A. J., … Vitart, F. (2011). The ERA-Interim reanalysis: Configuration and performance of the data assimilation system. *Quarterly Journal of the Royal Meteorological Society*, *137*(656), 553–597. https://doi.org/10.1002/qj.828

Di Lorenzo, E., Schneider, N., Cobb, K. M., Franks, P. J. S., Chhak, K., Miller, A. J., McWilliams, J. C., Bograd, S. J., Arango, H., Curchitser, E., Powell, T. M., & Rivière, P. (2008). North Pacific Gyre Oscillation links ocean climate and ecosystem change. *Geophysical Research Letters*, *35*(8). https://doi.org/10.1029/2007GL032838

Digital Research Alliance of Canada. (2022, October 6). https://alliancecan.ca/en/services/advanced-research-computing

Dosser, H. V., Waterman, S., Jackson, J. M., Hannah, C. G., Evans, W., & Hunt, B. P. V. (2021). Stark Physical and Biogeochemical Differences and Implications for Ecosystem Stressors in the Northeast Pacific Coastal Ocean. *Journal of Geophysical Research: Oceans*, *126*(11), e2020JC017033. https://doi.org/10.1029/2020JC017033

1010   Dosser, H. V., Waterman, S., Jackson, J. M., Hannah, C., & Hunt, B. P. V. (2020). *Tidal mixing maintains regional differences in water properties and nutrient ratios in British Columbia coastal waters* [Preprint]. Oceanography. https://doi.org/10.1002/essoar.10505244.1

Ebbesmeyer, C. C., Coomes, C. A., Cannon, G. A., & Bretschneider, D. E. (1989). Linkage of Ocean and Fjord Dynamics at Decadal Period. In D. H. Peterson (Ed.), *Aspects of Climate Variability*

1015   *in the Pacific and Western Americas* (pp. 399–417). American Geophysical Union (AGU). https://doi.org/10.1029/gm055p0399

Edwards, A., Tai, Travis, Watson, J., Peña, M. A., Hilborn, A., Hannah, C. G., Rooper, C. N., Flynn, K. L., & Oldford, G. (2024). *pacea: An R package of Pacific ecosystem information to help facilitate an ecosystem approach to fisheries management.* (Version v1.0.0) [Computer

1020   software]. Github / Zenodo. https://github.com/pbs-assess/pacea; https://doi.org/10.5281/zenodo.13840805

Environment and Climate Change Canada. (2020). *HRDPS data in GRIB2 format*. Environment & Climate Change Canada (ECCC). https://weather.gc.ca/grib/grib2_HRDPS_HR_e.html

Esenkulova, S., Suchy, K. D., Pawlowicz, R., Costa, M., & Pearsall, I. A. (2021). Harmful Algae and

1025   Oceanographic Conditions in the Strait of Georgia, Canada Based on Citizen Science Monitoring. *Frontiers in Marine Science*, *8*, 1193. https://doi.org/10.3389/FMARS.2021.725092/BIBTEX

Fatland, R., MacCready, P., & Oscar, N. (2016). Chapter 14—LiveOcean. In T. C. Vance, N. Merati, C. Yang, & M. Yuan (Eds.), *Cloud Computing in Ocean and Atmospheric Sciences* (pp. 277–

1030   296). Academic Press. https://doi.org/10.1016/B978-0-12-803192-6.00014-1

Feely, R., Doney, S., & Cooley, S. (2009). Ocean Acidification: Present Conditions and Future Changes in a High-CO2 World. *Oceanography, 22*(4), 36–47. https://doi.org/10.5670/oceanog.2009.95

Fisheries and Oceans Canada (DFO). (2024). *Marine Environmental Data Section Archive* [Dataset].

1035   Ecosystem and Oceans Science, Department of Fisheries and Oceans Canada. https://meds-sdmm.dfo-mpo.gc.ca

Fisheries, & Canada (DFO), O. (2022a, January 14). *British Columbia lightstation daily sea-surface temperature and salinity measurements, 1914 to present* (NaN). https://catalogue.cioospacific.ca/dataset/ca-cioos_654a4ece-7271-4f5a-ba60-

1040   b50a62dbd051?local=en

Fisheries, & Canada (DFO), O. (2022b, January 14). *Vertical profiles of seawater properties measured by Conductivity-Temperature-Depth loggers in British Columbia, Canada, 1965 to present* (NaN). https://catalogue.cioospacific.ca/dataset/ca-cioos_89aa45fc-7b42-426e-9293-e5703534bc4f?local=en

1045   Foreman, M. G. G., Crawford, W. R., Cherniawsky, J. Y., Henry, R. F., & Tarbotton, M. R. (2000). A high-resolution assimilating tidal model for the northeast Pacific Ocean. *Journal of Geophysical Research: Oceans*, *105*(C12), 28629–28651. https://doi.org/10.1029/1999JC000122

Fulton, E. A., Blanchard, J. L., Melbourne-Thomas, J., Plagányi, É. E., & Tulloch, V. J. D. D. (2019).

1050   Where the Ecological Gaps Remain, a Modelers' Perspective. *Frontiers in Ecology and Evolution*, *7*, 424. https://doi.org/10.3389/fevo.2019.00424

Gasset, N., Fortin, V., Dimitrijevic, M., Carrera, M., Bilodeau, B., Muncaster, R., Gaborit, É., Roy, G., Pentcheva, N., Bulat, M., Wang, X., Pavlovic, R., Lespinas, F., & Khedhaouiria, D. (2021). *A 10 km North American Precipitation and Land SurfaceReanalysis Based on the GEM*

1055   *Atmospheric Model* [Preprint]. Hydrometeorology/Modelling approaches. https://doi.org/10.5194/hess-2021-41

Georgia Strait Alliance. (2020). *About the Strait*. https://georgiastrait.org/issues/about-the-strait-2/

Gocic, M., & Trajkovic, S. (2013). Analysis of changes in meteorological variables using Mann-Kendall and Sen's slope estimator statistical tests in Serbia. *Global and Planetary Change*,

1060   *100*, 172–182. https://doi.org/10.1016/j.gloplacha.2012.10.014

Goldfeld, S. M., & Quandt, R. E. (1965). Some Tests for Homoscedasticity. *Journal of the American Statistical Association*, *60*(310), 539–547. https://doi.org/10.1080/01621459.1965.10480811

Gower, J., King, S., Statham, S., Fox, R., & Young, E. (2013). The malaspina dragon: A newly-discovered pattern of the early spring bloom in the strait of georgia, british columbia, canada. *Progress in Oceanography*, *115*, 181–188. https://doi.org/10.1016/j.pocean.2013.05.024

Groot, G. & Margolis, L. (1991). *Pacific salmon life histories*. UBC press.

Gruber, N., Boyd, P. W., Frölicher, T. L., & Vogt, M. (2021). Biogeochemical extremes and compound events in the ocean. *Nature*, *600*(7889), Article 7889. https://doi.org/10.1038/s41586-021-03981-7

Guan, L. (2015). *Spatial and temporal dynamics of larval fish assemblages in the Strait of Georgia*. 159.

Harris, C. R., Millman, K. J., van der Walt, S. J., Gommers, R., Virtanen, P., Cournapeau, D., Wieser, E., Taylor, J., Berg, S., Smith, N. J., Kern, R., Picus, M., Hoyer, S., van Kerkwijk, M. H., Brett, M., Haldane, A., del Río, J. F., Wiebe, M., Peterson, P., … Oliphant, T. E. (2020). Array programming with NumPy. *Nature*, *585*(7825), 357–362. https://doi.org/10.1038/s41586-020-2649-2

Harrison, P. J., Fulton, J. D., Taylor, F. J. R., Parsons, T. R., Futon, J. E., & Taylor, F. J. R. (1983). Review of the Biological Oceanography of the Strait of Georgia: Pelagic Environment. *Canadian Journal of Fisheries and Aquatic Sciences*, *40*(7), 1064–1094. https://doi.org/10.1139/f83-129

Healey, M. C. (1980). The ecology of juvenile salmon in Georgia Strait, British Columbia. In *Salmonid ecosystems of the North Pacific.* (pp. 203–229). http://sogdatacentre.ca/bibtexbrowser.php?key=RefWorks%3A7713&bib=sog.bib

Helsel, D. R., & Hirsch, R. M. (1992). *Statistical methods in water resources* (Vol. 49). Elsevier. https://books.google.com/books?hl=en&lr=&id=jao4o5X1pvgC&oi=fnd&pg=PP2&dq=Statistical+Methods+in+Water+Resources&ots=QXPE8NicM_&sig=YwQK5vi1wBSQTPzHaMQl9hyLPYw

Hermann, A. J., Cheng, W., Stabeno, P. J., Pilcher, D. J., Kearney, K. A., & Holsman, K. K. (2023). Applications of Biophysical Modeling to Pacific High-Latitude Ecosystems. *Oceanography*, *36*(2/3), 101–108.

Hernández-Carrasco, I., Alou-Font, E., Dumont, P.-A., Cabornero, A., Allen, J., & Orfila, A. (2020). Lagrangian flow effects on phytoplankton abundance and composition along filament-like structures. *Progress in Oceanography*, *189*, 102469. https://doi.org/10.1016/j.pocean.2020.102469

1095 Hersbach, H., Bell, B., Berrisford, P., Hirahara, S., Horányi, A., Muñoz-Sabater, J., Nicolas, J., Peubey, C., Radu, R., Schepers, D., Simmons, A., Soci, C., Abdalla, S., Abellan, X., Balsamo, G., Bechtold, P., Biavati, G., Bidlot, J., Bonavita, M., … Thépaut, J. N. (2020). The ERA5 global reanalysis. *Quarterly Journal of the Royal Meteorological Society*, *146*(730), 1999–2049. https://doi.org/10.1002/qj.3803

1100 Ianson, D., Allen, S. E., Moore-Maley, B. L., Johannessen, S. C., & Macdonald, and Robie W. (2016). Vulnerability of a semienclosed estuarine sea to ocean acidification in contrast with hypoxia. *Geophysical Research Letters*, *43*(11), 5793–5801. https://doi.org/10.1002/2016GL068996

Islam, S. U., Hay, R. W., Déry, S. J., & Booth, B. P. (2019). Modelling the impacts of climate change on riverine thermal regimes in western Canada's largest Pacific watershed. *Scientific Reports*,
1105 *9*(1), Article 1. https://doi.org/10.1038/s41598-019-47804-2

Jackson, J. M., Barrette, J., & Hakai Institute. (2021, December 14). *Hakai Water Properties Vertical Profile Data Measured by Oceanographic Profilers, Research*.

Jackson, J. M., Bianucci, L., Hannah, C. G., Carmack, E. C., & Barrette, J. (2021). Deep Waters in British Columbia Mainland Fjords Show Rapid Warming and Deoxygenation From 1951 to
1110 2020. *Geophysical Research Letters*, *48*(3), e2020GL091094. https://doi.org/10.1029/2020GL091094

Jarníková, T., Ianson, D., Allen, S. E., Shao, A. E., & Olson, E. M. (2022). Anthropogenic Carbon Increase has Caused Critical Shifts in Aragonite Saturation Across a Sensitive Coastal System. *Global Biogeochemical Cycles*, *36*(7), e2021GB007024.
1115 https://doi.org/10.1029/2021GB007024

Johannessen, S. C., Macdonald, R. W., & Strivens, J. E. (2020). Has primary production declined in the Salish Sea? *Canadian Journal of Fisheries and Aquatic Sciences*, *250*, 363–6310. https://doi.org/10.1139/cjfas-2020-0115

Johannessen, S. C., Masson, D., & Macdonald, R. W. (2014). Oxygen in the deep Strait of Georgia,

1120   1951–2009: The roles of mixing, deep-water renewal, and remineralization of organic carbon.

        Limnology and Oceanography, *59*(1), 211–222. https://doi.org/10.4319/lo.2014.59.1.0211

Jones, A. R., Hosegood, P., Wynn, R. B., De Boer, M. N., Butler-Cowdry, S., & Embling, C. B. (2014).

        Fine-scale hydrodynamics influence the spatio-temporal distribution of harbour porpoises at a

        coastal hotspot. *Progress in Oceanography*, *128*, 30–48.

1125   https://doi.org/10.1016/j.pocean.2014.08.002

Kärnä, T., Ljungemyr, P., Falahat, S., Ringgaard, I., Axell, L., Korabel, V., Murawski, J., Maljutenko,

        I., Lindenthal, A., Jandt-Scheelke, S., Verjovkina, S., Lorkowski, I., Lagemaa, P., She, J.,

        Tuomi, L., Nord, A., & Huess, V. (2021). Nemo-Nordic 2.0: Operational marine forecast model

        for the Baltic Sea. *Geoscientific Model Development*, *14*(9), 5731–5749.

1130   https://doi.org/10.5194/gmd-14-5731-2021

Kendall, M. G. (1948). *Rank correlation methods.*

Khangaonkar, T., Nugraha, A., Lakshitha, P., Keister, J. E., & Borde, A. (2021). Projections of algae,

        eelgrass, and zooplankton ecological interactions in the inner Salish Sea – for future climate

        and altered oceanic states. *Accepted with Minor Revision, Journal of Ecological Modeling*,

1135   *441*, 109420. https://doi.org/10.1016/j.ecolmodel.2020.109420

Khangaonkar, T., Nugraha, A., Xu, W., & Balaguru, K. (2019). Salish Sea Response to Global

        Climate Change, Sea Level Rise, and Future Nutrient Loads. *Journal of Geophysical

        Research: Oceans*, *124*(6), 3876–3904. https://doi.org/10.1029/2018JC014670

Khangaonkar, T., Nugraha, A., Yun, S. K., Premathilake, L., Keister, J. E., & Bos, J. (2021).

1140   Propagation of the 2014–2016 Northeast Pacific Marine Heatwave Through the Salish Sea.

        Frontiers in Marine Science, *8*. https://doi.org/10.3389/fmars.2021.787604

Khangaonkar, T., Sackmann, B., Long, W., Mohamedali, T., & Roberts, M. (2012). Simulation of

        annual biogeochemical cycles of nutrient balance, phytoplankton bloom(s), and DO in Puget

        Sound using an unstructured grid model. *Ocean Dynamics 2012 62:9*, *62*(9), 1353–1379.

1145   https://doi.org/10.1007/S10236-012-0562-4

Levier, B., Tréguier, A.-M., Madec, G., & Garnier, V. (2007). *Free surface and variable volume in the NEMO code*. https://zenodo.org/records/3244182

Libralato, S., & Solidoro, C. (2009). Bridging biogeochemical and food web models for an End-to-End representation of marine ecosystem dynamics: The Venice lagoon case study. *Ecological Modelling*, *220*(21), 2960–2971.

Loarie, S. R., Duffy, P. B., Hamilton, H., Asner, G. P., Field, C. B., & Ackerly, D. D. (2009). The velocity of climate change. *Nature*, *462*(7276), 1052–1055. https://doi.org/10.1038/nature08649

MacCready, P., McCabe, R. M., Siedlecki, S. A., Lorenz, M., Giddings, S. N., Bos, J., Albertson, S., Banas, N. S., & Garnier, S. (2021). Estuarine Circulation, Mixing, and Residence Times in the Salish Sea. *Journal of Geophysical Research: Oceans*, *126*(2), e2020JC016738. https://doi.org/10.1029/2020JC016738

Macias, D., Garcia-Gorriz, E., Piroddi, C., & Stips, A. (2014). Biogeochemical control of marine productivity in the Mediterranean Sea during the last 50 years. *Global Biogeochemical Cycles*, *28*(8), 897–907.

Madec, G., Bell, M., Blaker, A., Bricaud, C., Bruciaferri, D., Castrillo, M., Calvert, D., Chanut, J., Clementi, E., Coward, A., Epicoco, I., Éthé, C., Ganderton, J., Harle, J., Hutchinson, K., Iovino, D., Lea, D., Lovato, T., Martin, M., … Wilson, C. (2023). *NEMO Ocean Engine Reference Manual*. https://doi.org/10.5281/zenodo.8167700

Madec, G., Bourdallé-Badie, R., Bouttier, P.-A., Bricaud, C., Bruciaferri, D., Calvert, D., Chanut, J., Clementi, E., Coward, A., Delrosso, D., Ethé, C., Flavoni, S., Graham, T., Harle, J., Iovino, D., Lea, D., Lévy, C., Lovato, T., Martin, N., … Vancoppenolle, M. (2017). *NEMO ocean engine*. http://hdl.handle.net/2122/13309

Mann, H. B. (1945). Nonparametric Tests Against Trend. *Econometrica*, *13*(3), 245–259. https://doi.org/10.2307/1907187

Mantua, N. J., & Hare, S. R. (2002). The Pacific Decadal Oscillation. *Journal of Oceanography*, *58*(1), 35–44. https://doi.org/10.1023/A:1015820616384

Mantua, N. J., Hare, S. R., Zhang, Y., Wallace, J. M., & Francis, R. C. (1997). A Pacific Interdecadal Climate Oscillation with Impacts on Salmon Production. *Bulletin of the American Meteorological Society*, *78*(6), 1069–1079. https://doi.org/10.1175/1520-0477(1997)078<1069:APICOW>2.0.CO;2

Martins, E. G., Hinch, S. G., Patterson, D. A., Hague, M. J., Cooke, S. J., Miller, K. M., Lapointe, M. F., English, K. K., & Farrell, A. P. (2011). Effects of river temperature and climate warming on stock-specific survival of adult migrating Fraser River sockeye salmon (Oncorhynchus nerka). *Global Change Biology*, *17*(1), 99–114. https://doi.org/10.1111/j.1365-2486.2010.02241.x

Masson, D. (2002). Deep Water Renewal in the Strait of Georgia. *Estuarine, Coastal and Shelf Science*, *54*(1), 115–126. https://doi.org/10.1006/ecss.2001.0833

Masson, D., & Cummins, P. F. (2007). Temperature trends and interannual variability in the Strait of Georgia, British Columbia. *Continental Shelf Research*, *27*(5), 634–649.

Masson, D., & Peña, A. (2009). Chlorophyll distribution in a temperate estuary: The Strait of Georgia and Juan de Fuca Strait. *Estuarine, Coastal and Shelf Science*, *82*(1), 19–28. https://doi.org/10.1016/j.ecss.2008.12.022

McPhaden, M. J., Zebiak, S. E., & Glantz, M. H. (2006). ENSO as an Integrating Concept in Earth Science. *Science*, *314*(5806), 1740–1745. https://doi.org/10.1126/science.1132588

Melnychuk, M. C., Christensen, V., & Walters, C. J. (2013). Meso-scale movement and mortality patterns of juvenile coho salmon and steelhead trout migrating through a coastal fjord. *Environmental Biology of Fishes*, *96*(2–3), 325–339. https://doi.org/10.1007/s10641-012-9976-6

Melnychuk, M. C., Welch, D. W., & Walters, C. J. (2010). Spatio-temporal migration patterns of Pacific Salmon smolts in rivers and coastal marine waters. *PLoS ONE*, *5*(9), e12916. https://doi.org/10.1371/journal.pone.0012916

Miller, K. M., Teffer, A., Tucker, S., Li, S., Schulze, A. D., Trudel, M., Juanes, F., Tabata, A., Kaukinen, K. H., Ginther, N. G., Ming, T. J., Cooke, S. J., Hipfner, J. M., Patterson, D. A., & Hinch, S. G. (2014). Infectious disease, shifting climates, and opportunistic predators:

1200 Cumulative factors potentially impacting wild salmon declines. *Evolutionary Applications*, *7*(7), 812–855. https://doi.org/10.1111/eva.12164

Millero, F. (2010). History of the Equation of State of Seawater. *Oceanography*, *23*(3), 18–33. https://doi.org/10.5670/oceanog.2010.21

Moore, S. K., Johnstone, J. A., Banas, N. S., & Salathé, E. P. (2015). Present-day and future climate

1205 pathways affecting Alexandrium blooms in Puget Sound, WA, USA. *Harmful Algae*, *48*, 1–11. https://doi.org/10.1016/j.hal.2015.06.008

Morrison, J., Foreman, M. G. G., & Masson, D. (2012). A method for estimating monthly freshwater discharge affecting British Columbia coastal waters. *Atmosphere-Ocean*, *50*(1), 1–8.

Morrison, J., Quick, M. C., & Foreman, M. G. G. (2002). Climate change in the Fraser River

1210 watershed: Flow and temperature projections. *Journal of Hydrology*, *263*(1–4), 230–244.

NOAA National Buoy Data Centre. (2023). *Meteorological and oceanographic data collected from the National Data Buoy Center Coastal-Marine Automated Network (C-MAN) and moored (weather) buoys* [Dataset]. NOAA National Centers for Environmental Information. ttps://www.ncei.noaa.gov/archive/accession/NDBC-CMANWx

1215 Oldford, G. (2024a). *HOTSSea Model v1.02 monthly outputs* (Version 1.02.1) [Dataset]. Zenodo. https://doi.org/10.5281/zenodo.13871970

Oldford, G. (2024b). *goldford/HOTSSea_v1_NEMOandSupportCode: HOTSSea v1 Code for GMD-2024-58 v2* (Version 0.1.1) [Computer software]. Zenodo. https://zenodo.org/doi/10.5281/zenodo.12520930

1220 Oldford, G., & Dunphy, M. (2024a). *HOTSSea Forcings—HRDPS* (Dataset 10.5281/zenodo.12193923). https://doi.org/10.5281/zenodo.12193923

Oldford, G., & Dunphy, M. (2024b). *HOTSSea Forcings—RDRS v2.1* (Dataset 10.5281/zenodo.12206290.). Zenodo.org. https://doi.org/10.5281/zenodo.12206290.

Oldford, G., & Dunphy, M. (2024c). *HOTSSea v1 Forcings—CIOPSW, ERA5, ORAS5, Obs, Runoff*

1225 *etc* (Dataset 10.5281/zenodo.12312768). Zenodo.org. https://doi.org/10.5281/zenodo.12312768

Olson, E. M., Allen, S. E., Do, V., Dunphy, M., & Ianson, D. (2020). Assessment of Nutrient Supply by a Tidal Jet in the Northern Strait of Georgia Based on a Biogeochemical Model. *Journal of Geophysical Research: Oceans*, *125*(8), 1–25. https://doi.org/10.1029/2019jc015766

Pacific Salmon Foundation. (2022). *Digital elevation model for the Salish Sea at a resolution of 80 metres*. Marine Data BC. https://soggy2.zoology.ubc.ca:8443/geonetwork/srv/eng/catalog.search#/metadata/6b05c683-10f5-44fe-9983-7914e5cf0c72

Pacific Salmon Foundation. (2023). *Citizen Science Program*. Citizen Science Program. https://soggy2.zoology.ubc.ca/geonetwork/srv/eng/catalog.search#/metadata/ab455d82-59c5-4d8a-9c9f-bbc9636144b5

Paquin, J. P., Lu, Y., Smith, G., Taylor, S., Blanken, H., Lei, J., Dupont, F., Roy, F., Bernier, N., Marcotte, G., Davidson, F., Holden, J., Babalola, S., Sutherland, G., Zhai, L., Hu, X., Horwitz, R., Clainche, Y. L., Allen, S., … Jackson, J. (2020). CIOPS West: An operational forecasting model for oceans off Canada's west coast. *Ocean Predict 19*.

Parzen, E. (1964). An approach to empirical time series analysis. *Radio Science*, *68*(9), 937–951.

Pata, P. R., Galbraith, M., Young, K., Margolin, A. R., Perry, R. I., & Hunt, B. P. V. (2022). Persistent zooplankton bioregions reflect long-term consistency of community composition and oceanographic drivers in the NE Pacific. *Progress in Oceanography*, *206*, 102849. https://doi.org/10.1016/j.pocean.2022.102849

Pauly, D. (2021). The gill-oxygen limitation theory (GOLT) and its critics. *Science Advances*, *7*(2), eabc6050. https://doi.org/10.1126/sciadv.abc6050

Pauly, D., & Cheung, W. W. L. (2018). Sound physiological knowledge and principles in modeling shrinking of fishes under climate change. *Global Change Biology*, *24*(1), e15–e26. https://doi.org/10.1111/gcb.13831

Pawlowicz, R., Hannah, C., & Rosenberger, A. (2019). Lagrangian observations of estuarine residence times, dispersion, and trapping in the Salish Sea. *Estuarine, Coastal and Shelf Science*, *225*, 106246. https://doi.org/10.1016/j.ecss.2019.106246

Pearsall, A. I., Schmidt, M., Kemp, I., & Riddell, B. (2021). *Factors Limiting Survival of Juvenile Chinook Salmon, Coho Salmon and Steelhead in the Salish Sea: Synthesis of Findings of the Salish Sea Marine Survival Project*.

Peña, M. A., Masson, D., & Callendar, W. (2016). Annual plankton dynamics in a coupled physical—Biological model of the Strait of Georgia, British Columbia. *Progress in Oceanography*, *146*, 58–74.

Perry, I. (2021). Vignette 2: Lower Trophic Levels in the Salish Sea. *State of the Salish Sea*, 44. https://doi.org/10.25710/vfhb-3a69

Piroddi, C., Akoglu, E., Andonegi, E., Bentley, J. W., Celić, I., Coll, M., Dimarchopoulou, D., Friedland, R., de Mutsert, K., Girardin, R., Garcia-Gorriz, E., Grizzetti, B., Hernvann, P. Y., Heymans, J. J., Müller-Karulis, B., Libralato, S., Lynam, C. P., Macias, D., Miladinova, S., … Tsikliras, A. C. (2021). Effects of Nutrient Management Scenarios on Marine Food Webs: A Pan-European Assessment in Support of the Marine Strategy Framework Directive. *Frontiers in Marine Science*, *8*(March), 1–18. https://doi.org/10.3389/fmars.2021.596797

Potisomporn, P., Adcock, T. A. A., & Vogel, C. R. (2023). Evaluating ERA5 reanalysis predictions of low wind speed events around the UK. *Energy Reports*, *10*, 4781–4790. https://doi.org/10.1016/j.egyr.2023.11.035

Preikshot, D. B. (2007). The influence of geographic scale, climate and trophic dynamics upon North Pacific oceanic ecosystem models. [University of British Columbia]. In *PhD Dissertation*. http://ezproxy.library.ubc.ca/login?url=http://search.proquest.com/docview/20318385?accounti d=14656%5Cnhttp://gw2jh3xr2c.search.serialssolutions.com/?ctx_ver=Z39.88-2004&ctx_enc=info:ofi/enc:UTF-8&rfr_id=info:sid/ProQ&rft_val_fmt=info:ofi/fmt:kev:mtx:jour

Riche, O., Johannessen, S. C., & Macdonald, R. W. (2014). Why timing matters in a coastal sea: Trends, variability and tipping points in the Strait of Georgia, Canada. *Journal of Marine Systems*, *131*, 36–53.

Riddell, B., Brodeur, R. D., Bugaev, A. V., Moran, P., Murphy, J. M., Orsi, J. A., Trudel, M., Weitkamp, L. A., Wells, B. K., & Wertheimer, A. C. (2018). Ocean ecology of Chinook salmon. In R. J.

Beamish (Ed.), *Ocean Ecology of Pacific Salmon and Trout* (First Edit, pp. 555–696). American Fisheries Society.

Rose, K. A. (2012). End-to-end models for marine ecosystems: Are we on the precipice of a significant advance or just putting lipstick on a pig? *Scientia Marina*, *76*(1), 195–201.
1285 https://doi.org/10.3989/scimar.03574.20B

Rose, K. A., Allen, J. I., Artioli, Y., Barange, M., Blackford, J., Carlotti, F., Creekmore, S., Cropp, R., Daewel, U., Edwards, K., Flynn, K., Hill, S. L., HilleRisLambers, R., Huse, G., Mackinson, S., Mergrey, B., Moll, A., Rivkin, R., Salihoglu, B., … Zhou, M. (2010). End-To-End Models for the Analysis of Marine Ecosystems: Challenges , Issues , and Next Steps. *Marine and Coastal*
1290 *Fisheries: Dynamics, Management, and Ecosystem Science*, *2*, 115–130. https://doi.org/10.1577/C09-059.1

Schulzweida, U. (2022). *CDO User Guide*. https://doi.org/10.5281/ZENODO.7112925

Seabold, S., & Perktold, J. (2010). *Statsmodels: Econometric and Statistical Modeling with Python*. 92–96. https://doi.org/10.25080/Majora-92bf1922-011

1295 Sen, P. K. (1968). Estimates of the Regression Coefficient Based on Kendall's Tau. *Journal of the American Statistical Association*, *63*(324), 1379–1389. https://doi.org/10.1080/01621459.1968.10480934

Shapiro, S. S., & Wilk, M. B. (1965). An Analysis of Variance Test for Normality (Complete Samples). *Biometrika*, *52*(3/4), 591–611. https://doi.org/10.2307/2333709

1300 Sharma, R., Vélez-Espino, L. A., Wertheimer, A. C., Mantua, N., & Francis, R. C. (2013). Relating spatial and temporal scales of climate and ocean variability to survival of Pacific Northwest Chinook salmon (Oncorhynchus tshawytscha). *Fisheries Oceanography*, *22*(1), 14–31. https://doi.org/10.1111/fog.12001

Snauffer, E. L., Masson, D., & Allen, S. E. (2014). Modelling the dispersal of herring and hake larvae
1305 in the Strait of Georgia for the period 2007-2009. *Fisheries Oceanography*, *23*(4), 375–388. https://doi.org/10.1111/fog.12072

Sobocinski, K. L., Greene, C. M., Anderson, J. H., Kendall, N. W., Schmidt, M. W., Zimmerman, M. S., Kemp, I. M., Kim, S., & Ruff, C. P. (2021). A hypothesis-driven statistical approach for

identifying ecosystem indicators of coho and Chinook salmon marine survival. *Ecological Indicators*, *124*, 107403. https://doi.org/10.1016/j.ecolind.2021.107403

Sobocinski, K. L., Kendall, N. W., Greene, C. M., & Schmidt, M. W. (2020). Ecosystem indicators of marine survival in Puget Sound steelhead trout. *Progress in Oceanography*, *188*, 102419. https://doi.org/10.1016/j.pocean.2020.102419

Soontiens, N., & Allen, S. E. (2017). Modelling sensitivities to mixing and advection in a sill-basin estuarine system. *Ocean Modelling*, *112*, 17–32. https://doi.org/10.1016/j.ocemod.2017.02.008

Soontiens, N., Allen, S. E., Latornell, D., Souëf, K. L., Paquin, J., Lu, Y., Thompson, K., Korabel, V., Soontiens, N., Allen, S. E., Latornell, D., Souëf, K. L., Paquin, J., Lu, Y., Thompson, K., Korabel, V., Surges, S., Soontiens, N., Allen, S. E., … Machuca, I. (2016). Storm Surges in the Strait of Georgia Simulated with a Regional Model. *Atmosphere-Ocean*, *54*(1–21). https://doi.org/10.1080/07055900.2015.1108899

Suchy, K. D., Young, K., Galbraith, M., Perry, R. I., & Costa, M. (2022). Match/Mismatch Between Phytoplankton and Crustacean Zooplankton Phenology in the Strait of Georgia, Canada. *Frontiers in Marine Science*, *9*. https://www.frontiersin.org/article/10.3389/fmars.2022.832684

Teffer, A. K., Bass, A. L., Miller, K. M., Patterson, D. A., Juanes, F., & Hinch, S. G. (2018). Infections, fisheries capture, temperature, and host responses: Multistressor influences on survival and behaviour of adult Chinook salmon. *The Ocean Tracking Network: Advancing Aquatic Research and Management*, *01*(01), 2069–2083. https://doi.org/10.1139/cjfas-2017-0491@cjfas-otn.issue01

Theil, H. (1950). A rank-invariant method of linear and polynominal regression analysis (Parts 1-3). *Ned. Akad. Wetensch. Proc. Ser. A*, *53*, 1397–1412.

Thomson, R. E., & Huggett, W. S. (1980). M2 Baroclinic Tides in Johnstone Strait, British Columbia. *Journal of Physical Oceanography*, *10*(10), 1509–1539. https://doi.org/10.1175/1520-0485(1980)010<1509:MBTIJS>2.0.CO;2

Tietsche, S., Alonso-Balmaseda, M., Zuo, H., & de Rosnay, P. (2017). Comparing Arctic winter sea-ice thickness from SMOS and ORAS5. *Technical Memorandum*, *803*.

https://www.ecmwf.int/en/elibrary/17275-comparing-arctic-winter-sea-ice-thickness-smos-and-oras5

Treasury Board Secretariat. (2023). *British Columbia Lightstation Sea-Surface Temperature and Salinity Data (Pacific), 1914-present—Open Government Portal*. British Columbia Lightstation Sea-Surface Temperature and Salinity Data (Pacific), 1914-Present. https://open.canada.ca/data/en/dataset/719955f2-bf8e-44f7-bc26-6bd623e82884

Trudel, M., Fisher, J., Orsi, J. A., Morris, J. F. T., Thiess, M. E., Sweeting, R. M., Hinton, S., Fergusson, E. A., & Welch, D. W. (2009). Distribution and Migration of Juvenile Chinook Salmon Derived from Coded Wire Tag Recoveries along the Continental Shelf of Western North America. *Transactions of the American Fisheries Society*, *138*(6), 1369–1391. https://doi.org/10.1577/t08-181.1

Trudel, M., & Tucker, S. (2013). Depth distribution of 1SW Chinook salmon in Quatsino Sound, British Columbia, during winter. *North Pacific Anadromous Fish Commission*, *1453*(1).

Tucker, S., Trudel, M., Welch, D. W., Candy, J. R., Morris, J. F. T., Thiess, M. E., Wallace, C., Teel, D. J., Crawford, W., Farley, E. V., & Beacham, T. D. (2009). Seasonal Stock-Specific Migrations of Juvenile Sockeye Salmon along the West Coast of North America: Implications for Growth. *Transactions of the American Fisheries Society*, *138*(6), 1458–1480. https://doi.org/10.1577/T08-211.1

Tuller, S. E. (2004). Measured wind speed trends on the west coast of Canada. *International Journal of Climatology: A Journal of the Royal Meteorological Society*, *24*(11), 1359–1374.

Virtanen, P., Gommers, R., Oliphant, T. E., Haberland, M., Reddy, T., Cournapeau, D., Burovski, E., Peterson, P., Weckesser, W., Bright, J., van der Walt, S. J., Brett, M., Wilson, J., Millman, K. J., Mayorov, N., Nelson, A. R. J., Jones, E., Kern, R., Larson, E., … Vázquez-Baeza, Y. (2020). SciPy 1.0: Fundamental algorithms for scientific computing in Python. *Nature Methods*, *17*(3), 261–272. https://doi.org/10.1038/s41592-019-0686-2

Walters, C. J., & Christensen, V. (2019). Effect of non-additivity in mortality rates on predictions of potential yield of forage fishes. *Ecological Modelling*, *410*(C), 1. https://doi.org/10.1016/j.ecolmodel.2019.

1365   Walters, C. J., Pauly, D., & Christensen, V. (1999). Ecospace: Prediction of Mesoscale Spatial

Patterns in Trophic Relationships of Exploited Ecosystems, with Emphasis on the Impacts of

Marine Protected Areas. *Ecosystems*, *2*, 539–554. https://doi.org/10.1007/s12009-000-0069-3

Water Survey of Canada. (2015). *Water Survey of Canada Historical Hydrometric Data*.

https://wateroffice.ec.gc.ca/search/historical_e.html

1370   Welch, D. W., Melnychuk, M. C., Payne, J. C., Rechisky, E. L., Porter, A. D., Jackson, G. D., Ward, B.

R., Vincent, S. P., Wood, C. C., & Semmens, J. (2011). In situ measurement of coastal ocean

movements and survival of juvenile Pacific salmon. *Proceedings of the National Academy of

Sciences of the United States of America*, *108*(21), 8708–8713.

https://doi.org/10.1073/pnas.1014044108

1375   White, H. (1980). A Heteroskedasticity-Consistent Covariance Matrix Estimator and a Direct Test for

Heteroskedasticity. *Econometrica*, *48*(4), 817–838. https://doi.org/10.2307/1912934

Wilcox, R. (1998). A Note on the Theil-Sen Regression Estimator When the Regressor Is Random

and the Error Term Is Heteroscedastic. *Biometrical Journal*, *40*(3), 261–268.

https://doi.org/10.1002/(SICI)1521-4036(199807)40:3<261::AID-BIMJ261>3.0.CO;2-V

1380   Willmott, C. J. (1981). On the Validation of Models. *Physical Geography*, *2*(2), 184–194.

https://doi.org/10.1080/02723646.1981.10642213

Yin, K., Goldblatt, R. H., Harrison, P. J., John, M. A. S., Clifford, P. J., Beamish, R. J., St. John, M. A.,

Clifford, P. J., & Beamish, R. J. (1997). Importance of wind and river discharge in influencing

nutrient dynamics and phytoplankton production in summer in the central Strait of Georgia.

1385   *Marine Ecology Progress Series*, *161*, 173–183. https://doi.org/10.3354/meps161173

Yue, S., Pilon, P., Phinney, B., & Cavadias, G. (2002). The influence of autocorrelation on the ability

to detect trend in hydrological series. *Hydrological Processes*, *16*(9), 1807–1829.

https://doi.org/10.1002/hyp.1095

Zaron, E. D. (2011). Introduction to Ocean Data Assimilation. In A. Schiller & G. B. Brassington

1390   (Eds.), *Operational Oceanography in the 21st Century* (pp. 321–350). Springer Netherlands.

https://doi.org/10.1007/978-94-007-0332-2_13

Zuo, H., Balmaseda, M. A., Tietsche, S., Mogensen, K., & Mayer, M. (2019). The ECMWF operational ensemble reanalysis-analysis system for ocean and sea ice: A description of the system and assessment. *Ocean Science*, *15*(3), 779–808. https://doi.org/10.5194/os-15-779-2019

1395